

We are grateful to the reviewers for their careful reading and very constructive comments. All points addressed by the reviewers have been taken into account in the revision of the manuscript.

Point-by point changes in the manuscript based on the reviewers' comments:

## REVIEWER #1

From the abstract and conclusion, it seems that the focus of this paper is on the response of African and Indian monsoon to precession and obliquity, but this is only briefly mentioned in several places and the analysis of processes was not done by this paper but was referred to other studies which have similar findings. The authors should stress what is new in the paper and its original contribution to interglacial and monsoon study.

**We have totally revised the abstract and conclusions following the reviewer's suggestion**

The conclusion of the authors that the global monsoon concept is challenged is actually based on the differences between 416kyr and 394kyr and between 495kyr and 516kyr where the precession is very similar between two time slices. It means that the role of precession is minimized in these comparisons. However, Fig10 tells that both Africa and Indian monsoon are mainly controlled by precession and both are highly and negatively correlated with precession. It means that at the astronomical time scale, both monsoon systems would co-vary with precession, and therefore the global monsoon concept could still be valid.

**Probably the manuscript was not clear enough regarding this point. The global monsoon concept is basically challenged by the time slices of 394 ka and 615 ka, where the North African rainfall anomaly has opposite sign compared to the Indian anomaly (see Table 2). This clearly points to the fact that the two regional monsoon systems do not always vary in concert.**

**We have revised the manuscript for clarification (Page 9, lines 762-769)**

In sections 3.1-3.6, it would be more interesting and add more value to the paper if the CCSM3 results are compared to proxy data and to other model results, even qualitatively. Moreover, in most of the discussions, only insolation has been used to explain the changes, and the role of CO<sub>2</sub> seems to have been forgotten.

**An in-depth model-data analysis is beyond the scope of this study. Several time slices from our set of experiments have already contributed to comprehensive model-data comparison (Lunt et al., 2013; Milker et al., 2013; Kleinen et al., 2014) and we refer to those studies. Comparison to other model studies is part of the discussion.**

**We have added several statements to discuss the role of GHG forcing (page 8, lines 709-716, page 7, lines 527-530, page 5, lines 375-377, page 5, lines 450-457, page 5, lines 362-367, page 9, lines 751-755)**

Specific comments:

1. Title: Not all the interglacials from MIS15 to MIS1 have been analyzed in this paper, so please be precise.

**We have changed the title to "Intra-interglacial climate variability: Model simulations of Marine Isotope Stages 1, 5, 11, 13, and 15"**

2. Please change everywhere "orbital" to "astronomical" because obliquity is not orbitally related.

**We have changed 'orbital' to 'astronomical' everywhere.**

3. Page 3037:

L1: for the periodicity of the astronomical parameters, Berger (1978, J.Atmos.Sci) deserves to be cited

**We have added Berger (1978) on page 1, line 52**

L1-4: about the influence of evolution of astronomical parameters on the internal structure of interglacials, I recommend the paper Yin and Berger (2015, QSR) to the authors.

**The reference has been included on page 1, lines 66-67**

L8-29: many interglacial simulations (both snapshot and transient) have been done in earlier time with both EMICs and GCMs, eg. Kubatzki et al (2000, Clim Dyn), Crucifix and Loutre (2002, Clim Dyn), Loutre and Berger (2003, global planetary change), Yin and Berger (2012, Clim Dyn) and Yin and Berger (2015, QSR). These deserve to be included in the introduction.

**These references have been included on page 1, lines 65-67**

L22-26: please specify what is the advantage of using realistic interglacial astronomical configurations as compared to the idealized astronomical forcing.

**We consider realistic and idealized forcing experiments equally important. Idealized experiments provide important insight into the climate system's response to astronomical forcing. However, since this response may be non-linear, using extreme values of astronomical parameters in idealized experiments tells us only a part of the story. Therefore, idealized and realistic forcing experiments should be considered complementary. Obviously, realistically forced experiments have a stronger potential for model-data comparison.**

**We added an explanation to the introduction (page 2, lines 125-133)**

4. In Section 3.1, 3.2 and 3.3, only insolation is used to explain the difference between the interglacials, but what is the role of CO<sub>2</sub>?

**Without individual forcing experiments as e.g. in Yin and Berger (2012) final conclusions about the role of CO<sub>2</sub> can not be drawn (given the computational expense of additional individual forcing experiments with the comprehensive CCSM3, such experiments are however beyond the scope of this study). We partly circumvent this problem by introducing the correlation maps in Section 3.6, which provide a hint on the importance of GHG forcing. However, for the individual seasons, we surmise that insolation forcing is dominant in most regions of the globe. CO<sub>2</sub> may play a larger role for the annual means (cf. Yin and Berger, 2012).**

**Nevertheless, we have added several statements to discuss the role of GHG forcing (see above).**

5. In section 3.1, please explain the southern ocean cooling in Group I. This is quite similar to the results of Yin and Berger (2012) where this cooling is attributed to summer remnant effect of local insolation.

**We have added an explanation on page 4, lines 308-311.**

6. Page3078, L15-17: is the cooling over southern hemisphere continents statistically significant? By the way, are the features given in fig3, 4, 5,6 significant?

**Yes, all colored responses are significant (t-test,  $p < 0.05$ ). Note that the maps were calculated from 100-yr means.**

7. Page3079:

L8: : : southern hemisphere (except Antarctica)

**Added on page 4, lines 340-341.**

Page3079, L19-23: are these observed in your model or in other study? The same processes have been demonstrated in Yin and Berger (2012) where the definition of “summer remnant effect” was given.

**We have observed the same processes as in previous studies and therefore cited Yin and Berger, 2012 on page 5, line 362.**

L24: I would add “probably” before “masked”.

**We have added ‘probably’ before ‘masked’ in page 5, line 365**

8. Page3080, L1-3: is it possible to give explanation about the temperature change?

**Low GHG concentrations play a role for the year-round extratropical cooling in this experiment. We have added a remark on page 5, lines 375-377.**

9. Page3081, L29-28: why does the JJAS warming over southern ocean and Antarctica not appear in 495-516? For 416-394, the summer remnant effect happens over the polar oceans, how to explain the warming over Antarctica continent and a cooling over western Antarctica? CO2 effect needs to be discussed here.

**We have added a discussion including the role of GHG on page 5, lines 445-457.**

10. Page3082:

L11: the effect of obliquity on annual insolation at high and low latitudes does not need to be implied, it is explicitly demonstrated in Berger et al (2010, QSR).

**We have rephrased this statement.**

L18-22: what is the role of lower CO2 at 495 than 516 to explain the weaker Sahel rainfall increase during MIS13 than during MIS-11?

**The GHG forcing is too small to exert a dominant effect on the Sahel rainfall change (cf. Figure 10). A more convincing argumentation will take the change in meridional insolation gradients into account, which is much larger in MIS11 than in MIS13.**

**We have added an explanation on page 6, lines 482-489.**

11. Section 3.6: how were the correlations made? Are these correlations statistically significant?

**We have added an additional explanation on page 6, lines 496-503.**

12. Page3083:Figure9a: why is the correlation between GHG and high latitude temperature very weak? This seems not consistent with the knowledge that high latitudes response to GHG change is much larger than the other part of the world.

**The correlation maps have to be interpreted carefully. Just because the correlation coefficients are small, this does not mean that GHG have no effect. The correlation is weak, because other forcings (obliquity, precession) have a much larger influence in our set of experiments, where GHG variations are relatively small.**

13. Page 3083: For the relative impact of obliquity and precession on surface temperature and precipitation, I recommend the paper Yin and Berger (2015, QSR) where results were obtained from transient simulations covering a large range of precession and obliquity.

**The reference has been included e.g. in the introduction.**

14. Page 3083, L15: how about the monsoon change in other Southern Hemisphere regions? **The effect on surface temperature is indeed smaller in South America and South Africa (overwhelmed by local TOA insolation anomalies), but still visible in the annual mean temperature.**

**We have added a sentence on page 7, lines 548-550.**

15. Page 3083, L17: in some doubling CO<sub>2</sub> experiments, it is shown that monsoon precipitation is sensitive to CO<sub>2</sub> change (eg. IPCC report), but in your figure 10a, there is no correlation between the two. Please explain

**Please note that the CO<sub>2</sub> variations are relatively small, i.e. far from being doubled. The effects of astronomical forcing on the monsoons are way larger than the relatively small GHG variations during the interglacials. Hence, the absence of a significant correlation in Figure 10a is reasonable.**

**We have added a sentence on page 7, lines 527-530.**

16. Page 3083, L23-24: how about the precession influence on the East Asian monsoon in your model?

**East Asian rainfall shows a somewhat heterogeneous pattern and is, in general, only weakly coupled with the Indian and African monsoons. This finding is consistent with a recent model intercomparison study by Dallmeyer et al. (Clim. Past, 11, 305-326, 2015) who found a stronger response of the North African and Indian monsoon systems to insolation forcing than of the East Asian monsoon.**

**We have added these sentences on page 7, lines 540-544.**

17. Page 3085:

L15-16: pay attention that the GHG and precession are not exactly the same between the time slices. **We agree and have been added a note/remark.**

**We have added a remark on page 7, lines 613-614.**

L26-29: the dating uncertainty and the tuning procedure of LR04 stack should not be ignored here in such discussion. Moreover, lag between climate forcing and ice sheet response should also been taken into account

**We have added a cautionary note on page 8, lines 639-640.**

18. Page 3086, L1-5: although 495kyr is the warmest in Group II, it is still much cooler than Pre-industrial in NH summer (fig3). How can you conclude that this cooling is not enough for ice sheet growth? In the simulation of Ganopolski and Calov (2011), there is a small ice sheet developed around 495 kyr

**We cannot provide a final conclusion without coupling the model to an ice sheet model. Our suggestion has to be considered a hypothesis.**

**We have rephrased the sentence on page 8, line 636 by using the word “hypothesize”**

19. Page 3087, L4-6: please demonstrate this statement

**This conclusion simply derives from the consideration of the two corresponding insolation maps of the 394 and 615 kyr experiments (see below), suggesting that the sensitivity of the tropical monsoons is not uniform: the North African monsoon is more sensitive to summer insolation while the Indian monsoon to spring-early summer insolation. Similar results have been found by Braconnot et al. (Climate of the Past 4, 281-294, doi:10.5194/cp-4-281-2008, 2008). It has been argued that the reason is a resonant response of the Indian monsoon to the insolation forcing when maximum insolation anomalies occur near the summer solstice and a resonant response of the African monsoon – which has its rainfall maximum one month later in the annual cycle than the Indian monsoon – when the maximum insolation change is delayed after the summer solstice.**

**We have added an explanation and the reference (Braconnot et al., 2008) on page 8, lines 684-691.**

20. Page 3087:

L16-17: please specify which is more important in controlling the Africa monsoon, precession or obliquity.

**Both are important, but the response to precession is still stronger.**

For clarification we have added a sentence on page 9, lines 760-762.

L21-23 and Page 3072, L15-17: These lines are not convincing, see my comment 18.  
We have rephrased the sentences on page 1, line 36, page 9, lines 778-780.

21. Page 3088, L8-9: I remind that transient simulations for earlier interglacials have been given in Yin and Berger (2015, QSR).

**We agree, but our statement only refers to CGCMs (i.e. general circulation models) and does not include EMICs.**

## REVIEWER #2

Main comments

A- Introduction. The introduction should be extended to provide more information. In particular, it would be useful to the reader to briefly discuss some main characteristics of the interglacials considered here, such as the length, the maximum temperature anomaly reconstructed compared to preindustrial and the relative sea level, if available. It should also be explained why the early Brunhes interglacials (MIS 13 and before) are different from the later interglacials, as later in the paper this is referred to. In addition, the main findings of previous modelling studies that have focused on several of the considered interglacials, should be briefly discussed. This is especially relevant for the Herold et al. (2012) study that was conducted with the same CCSM3 model. It should also be explained more clearly what the novelty of the present study is compared to these previous studies. This should include a rationale for selecting these specific interglacials and these 14 time slices, as this is not clear from the introduction.

**We have revised the introduction according to the reviewer's suggestions.**  
**Page 2, lines 82-85, page 2, lines 111-119, page 2, lines 89-109.**

B- Setup of experiments. Orbital forcing: The authors should discuss the season definition that they have used for the insolation in the different experiments (see Joussaume and Braconnot, 1997). I suspect that the date of vernal equinox has been kept fixed at today's value. The choice of calendar should be made clear, as it has potentially a huge impact on the results.

**We used a fixed calendar based on a 365 day year (the Day/Month values refer to the present calendar). We agree that a fixed calendar may affect the results, however, the strongest effects are known to occur in boreal fall, whereas the effect in boreal summer and winter (the seasons discussed in our manuscript) are small (e.g. Timm et al., *Paleoceanography*, 23, PA2221, 2008).**

**We have added an explanation on page 3, lines 194-199.**

C- Results. The results section could be improved, as the explanation of the results is in a few instances not very convincing.

On page 3079, line 15, the warm conditions in winter in the Arctic in the Group I experiments is discussed. "However, anomalously warm conditions in the Arctic stand in contrast to the global DJF cooling at 6, 9, 125, 405, and 416 kyr BP. The Arctic warming is due to the remnant effect of the polar summer insolation through ocean–sea ice feedbacks ". I wonder if this is the full explanation. Why is this Arctic winter warming not present in the other Group I simulations for 504 ka and 579 ka? For instance, looking at the insolation anomalies in Figure 2, the forcing looks very similar for 125k and 504 ka, but the Arctic warming in winter is absent in the simulation for 504 ka. Please elaborate

**The role of GHG forcing has to be taken into account, since in the early Brunhes time slices (504 and 579 ka) the low-GHG cooling masks the summer remnant effect in the Arctic.**

**We revised the text for clarification on page 5, lines 362-365.**

In Section 3.5 (page 3081), the effects of obliquity is discussed by comparing the anomalies of 416 minus 394 ka and 495 minus 516 ka. It is concluded on line 22 that in the 416 ka and 495 ka cases with maximum obliquity forcing, the boreal summer temperature in monsoon regions is lower than in the minimum obliquity cases because of higher rainfall. However, as can be seen in Figure 8f, the precipitation anomalies are very small (less than 0.2 mm/day) in monsoonal areas in the 495 ka case, making this conclusion highly unlikely, at least for 495 ka. I think it is more plausible that the negative insolation anomaly at low latitudes depicted in Figure 7 is the direct cause of the negative temperature anomaly. For the 495 ka case, the June-July insolation at 10\_N is more than 10 Wm<sup>-2</sup> less than in 516ka.

**The reviewer is absolutely right. Direct insolation forcing is the major cause for the low latitude cooling in the 495 ka experiment.**

**We have reformulated the paragraph on page 5, lines 439-442.**

At line 20, the small rainfall anomaly in the Sahel in the 495-516 ka plot (8f) is explained by the high precession at 495 ka which counteracted the obliquity-induced increase in monsoonal rainfall expected by the authors. This is an implausible explanation, as precession has similar values at 495 and 516 ka (Figure 1). However, even if precession values would have been different, the modelled climate does not "see" the high precession (or high obliquity), as it is only forced by the insolation anomalies that result from the changes in astronomical parameters. These insolation anomalies are shown in Figure 7. I think it is deceptive to consider variations in astronomical parameters as direct forcings of climate change in particular areas. Instead one should consider the net effect of these astronomical parameters on the insolation, which as a result varies per latitude and per month as is clear from Figure 7.

**We have added an explanation that takes the spatiotemporal insolation anomaly patterns shown in Figure 7 into account. Page 6, lines 482-489.**

D- Discussion and conclusions. The discussion should be extended to include several limitations of the study. As mentioned in the conclusions, the model experiments did not include appropriate ice sheet configurations, while it is known that changes in ice sheets also affected interglacial climates. The potential effect of prescribing preindustrial ice sheets should be properly discussed, and not just be mentioned in the conclusions. In fact, it is not a conclusion from this study.

**We have moved the corresponding paragraph from the Conclusions to the Discussion section plus a brief comment on uncertainties in ice-sheet reconstructions on page 8, lines 717-731.**

In addition, also the impact of the choice of calendar on the results should be discussed in Section 4. The conclusions should also stress more clearly what the added value of this study is compared to the various other recent modelling studies that have focused on interglacial climates. Do the experiments provide improved understanding of certain features seen in proxy-based reconstructions? If so, where?

**The effect of a fixed calendar is small for the considered seasons (summer, winter) as now mentioned in the revised Section 2.2, hence an additional discussion is not required. The Conclusions have been revised.**

Minor comments

Page 3074, line 24: "have usually set to extreme values" should be "have usually been set to extreme values".

**We have revised this on page 2, line 122.**

Page 3074, line 26: "our analyzes are based on realistic orbital configurations and hence climate states". I disagree with this statement. The fact that realistic orbital configurations are

prescribed does not necessarily mean that the simulated climate states are also realistic. For instance, preindustrial ice sheets have been prescribed in all experiments, while it is well known that there have been substantial changes in ice sheet configuration during the considered interglacials, which will have impacted the climate as well.

**We have removed 'and hence climate states' on page 2, line 125.**

Page 3075, line 6. Starting from the preindustrial spin-up, each experiment was run for 400 years, of which the last 100 years were used in the analysis. After 400 years, the deep ocean is still adjusting to the change in forcings (e.g. Renssen et al. 2006). For this reason, other similar studies have used a longer run time, for instance, 1000 years in Yin & Berger (2012) and Herold et al. (2012). Although in the present study the focus is on the surface climate, for which 400 years is probably sufficient, I would still suggest that to discuss this issue in Section 2.2.

**We have added a note on page 3, lines 182-186.**

Page 3080, line 6: I propose to rephrase this sentence (2x precipitation). "precipitation shown in Fig. 5 exhibits intensified precipitation: : :"

**We have replaced one of two 'precipitation on page 5, lines 379-380 to 'rainfall'.**

Page 3080, line 11: " The most interesting results regarding the tropical rainfall response to astronomical forcing appear in Group III, where the monsoonal precipitation anomalies show opposite signs in North Africa and India." This is the case for the 615k simulation, but it is not clear for the 394k experiment, as Figure 5 clearly shows for 394k enhanced precipitation in N Africa and India. Please revise.

**Figure 5 clearly shows reduced (yellow) precipitation in the North African Sahel region in the 394 ka experiment (enhanced precipitation is only visible in Central Africa).**

**We have added "Sahel region" for clarification on page 5 lines 389-390.**

Page 3080, line 25: "In high Arctic latitudes, vegetation advances (NPP increases) in the Group I simulations: : : " If NPP increases, does it necessarily reflect an advance of vegetation? It could also reflect a change of the vegetation at the site itself, couldn't it? I would say it is not so straightforward to interpret simulated NPP changes in terms of shifts in vegetation. But maybe the authors have also checked other output from their DGVM to come to their interpretation. If this is the case, I suggest explaining this in the manuscript. The same is true for the NPP decline in the Arctic in the Group II simulations.

**We agree and have rephrased the sentence on page 5 lines 406-409.**

Page 3082, Section 3.6. I would propose to explain in more detail how the correlation maps are constructed and what they mean. The values of the GHG forcing are not necessarily independent from the values of precession and obliquity. For instance, CO<sub>2</sub> and CH<sub>4</sub> levels in the atmosphere depend on exchange between carbon pools, which in turn is affected by climate due to changes in astronomical parameters. So if there is a positive correlation of temperature with GHG forcing, we are not purely looking at correlation to the radiative forcing, but potentially also at the correlation to orbital forcing in the background. What does the correlation to GHG radiative forcing mean, and how should it be compared to the correlation with precession and obliquity?

**GHG forcing and astronomical parameters are not significantly correlated in our set of experiments, hence the reviewer's point is not an issue.**

**To explain the construction of the correlation maps we have added an additional paragraph on page 6, lines 496-503.**

Page 3088, line 12. I do not consider CCSM3 a "state-of-the-art" model, as it was released more than 10 years ago. We have already the next generation: CCSM4 (and CESM).

**We have removed 'state-of-the-art' on page 8, line 733 and replaced it with CCSM3-DGVM.**

# Intra-interglacial climate variability: Model simulations of Marine Isotope Stages 1, 5, 11, 13, and 15

Rima Rachmayani<sup>1</sup>, Matthias Prange<sup>1,2</sup>, and Michael Schulz<sup>1,2</sup>

<sup>1</sup>Faculty of Geosciences, University of Bremen, Klagenfurter Strasse, D-28334 Bremen, Germany

<sup>2</sup>MARUM - Center for Marine Environmental Sciences, University of Bremen, Leobener Strasse, D-28359 Bremen, Germany

1 Using the Community Climate System Model version 3  
2 (CCSM3) including a dynamic global vegetation model a set  
3 of 13 time slice experiments was carried out to study global  
4 climate variability between and within the Quaternary inter-  
5 glacial of Marine Isotope Stages (MIS) 1, 5, 11, 13, and 15.  
6 The selection of interglacial time slices was based on differ-  
7 ent aspects of inter- and intra-interglacial variability and as-  
8 sociated astronomical forcing. The different effects of obliquity,  
9 precession and greenhouse gas (GHG) forcing on global  
10 surface temperature and precipitation fields are illuminated.  
11 In most regions seasonal surface temperature anomalies can  
12 largely be explained by local insolation anomalies induced  
13 by the astronomical forcing. Climate feedbacks, however,  
14 may modify the surface temperature response in specific re-  
15 gions, most pronounced in the monsoon domains and the polar  
16 oceans. GHG forcing may also play an important role for  
17 seasonal temperature anomalies, especially in high latitudes  
18 and early Brunhes interglacials (MIS 13 and 15) when GHG  
19 concentrations were much lower than during the later inter-  
20 glacial. High-versus-low obliquity climates are generally  
21 characterized by strong warming over the Northern Hemi-  
22 sphere extratropics and slight cooling in the tropics during  
23 boreal summer. During boreal winter, a moderate cooling  
24 over large portions of the Northern Hemisphere continents  
25 and a strong warming at high southern latitudes is found.  
26 Beside the well-known role of precession, a significant role  
27 of obliquity in forcing the West African monsoon is identified.  
28 Other regional monsoon systems are less sensitive or  
29 not sensitive at all to obliquity variations during interglacials.  
30 Moreover, based on two specific time slices (394 and 615 kyr  
31 BP) it is explicitly shown that the West African and Indian  
32 monsoon systems do not always vary in concert, challeng-  
33 ing the concept of a global monsoon system at astronomical  
34 timescales. High obliquity can also explain relatively warm  
35 Northern Hemisphere high-latitude summer temperatures de-  
36 spite maximum precession around 495 kyrBP (MIS 13). It is

hypothesized that this obliquity-induced high-latitude warm-  
ing may have prevented a glacial inception at that time.

## 1 Introduction

The Quaternary period is characterized by the cyclic growth and decay of continental ice sheets associated with global environmental changes (e.g., Lisiecki and Raymo, 2005; Tzedakis et al., 2006; Jouzel et al., 2007; Lang and Wolff, 2011). While it is commonly accepted that the transitions between glacial and interglacial stages are ultimately triggered by varying astronomical insolation forcing (Hays et al., 1976), climate research is just beginning to understand the internal climate feedbacks that are required to shift the Earth system from one state to the other (e.g., van Nes et al., 2015). The astronomical forcing, with its characteristic periods of ca. 400 and 100 kyr (eccentricity), 41 kyr (obliquity), and ca. 19 and 23 kyr (precession) as in Berger (1978), also acts as an external driver for long-term climate change within the interglacials (i.e. the long-term intra-interglacial climate variability) and likely contributes to interglacial diversity since the evolution of astronomical parameters differs between all Quaternary interglacial stages (cf. Tzedakis et al., 2009; Yin and Berger, 2015). Understanding both interglacial climate diversity and intra-interglacial variability helps to estimate the sensitivity of the Earth system to different forcings and to assess the rate and magnitude of current climate change relative to natural variability.

Numerous interglacial climate simulations have been performed in previous studies using Earth system models of intermediate complexity (e.g., Kubatzki et al., 2000; Crucifix and Loutre, 2002; Loutre and Berger, 2003; Yin and Berger, 2012, 2015). While the present and the last interglacial have also been extensively investigated with fully coupled atmosphere-ocean general circulation models (e.g., Braconnot et al., 2007; Lunt et al., 2013), earlier interglacial periods have received much less attention by climate modellers. Coupled general circulation model (CGCM) studies of ear-



73 lier interglacial climates have recently been performed for 128  
 74 Marine Isotope Stage (MIS) 11 (Milker et al., 2013; Kleinen 129  
 75 et al., 2014) and MIS 13 (Muri et al., 2013). Using the 130  
 76 CGCM CCSM3 (Community Climate System Model version 131  
 77 3), Herold et al. (2012) presented a set of interglacial climate 132  
 78 simulations comprising the interglaciations of MIS 1, 5, 9, 133  
 79 11 and 19. Their study, however, focussed on peak inter- 134  
 80 glacial forcing (i.e. Northern Hemisphere summer occurring 135  
 81 at perihelion) and intercomparison of interglacials (i.e. inter- 136  
 82 glacial diversity) only. In particular, they found that, com- 137  
 83 pared to the other interglacials, MIS 11 exhibits the closest 138  
 84 resemblance to the present interglacial, especially during bo-  
 85 real summer.

86 Here, we present a different and complementary CGCM 139  
 87 (CCSM3) study which takes intra-interglacial climate vari- 140  
 88 ability into account by simulating two or more time slices 141  
 89 for each interglacial stage of MIS 1, 5, 11, 13, and 15. For 142  
 90 the interglacial of MIS 5 (Last Interglacial, MIS 5e; ca. 130- 143  
 91 115 kyr ago), proxy data suggest a peak global mean tem- 144  
 92 perature of about 1° C higher than during the pre-industrial 145  
 93 period (e.g., Otto-Bliesner et al., 2013; Dutton et al., 2015). 146  
 94 The maximum global mean sea-level has been estimated to 147  
 95 6–9 m above the present-day level (Kopp et al., 2009; Dutton 148  
 96 and Lambeck, 2012; Dutton et al., 2015). The interglacial of 149  
 97 MIS 11 was unusually long, about 30,000 years (ca. 425–395 150  
 98 kyr ago). Global average temperatures of MIS 11 are highly 151  
 99 uncertain, but a peak global mean temperature of up to 2° C 152  
 100 relative to pre-industrial cannot be ruled out (Lang and Wolff, 153  
 101 2011; Dutton et al., 2015). Maximum global mean sea-level 154  
 102 may have been 6–13 m higher than today (Raymo and Mitro- 155  
 103 vica, 2012; Dutton et al., 2015). Interglacials before MIS 11 156  
 104 (early Brunhes interglacials), like MIS 13 and 15, are gener- 157  
 105 ally characterized by lower global mean temperatures, larger 158  
 106 continental ice-sheets, lower global sea level and lower atmo- 159  
 107 spheric greenhouse gas (GHG) concentrations relative to the 160  
 108 more recent interglacials (e.g., Yin and Berger, 2010; Lang 161  
 109 and Wolff, 2011; Dutton et al., 2015).

110 The goal of this study is to disentangle the effects of obliqu- 162  
 111 uity, precession and GHG on global surface climate. Our 163  
 112 selection of interglacial time slices takes into account dif- 164  
 113 ferent aspects of inter- and intra-interglacial variability and 165  
 114 associated astronomical forcing. As such, our approach dif- 166  
 115 fers from and complements previous model studies that fo- 167  
 116 cussed on peak interglacial forcing and intercomparison of 168  
 117 interglacials (Yin and Berger, 2012; Herold et al., 2012). The 169  
 118 selection of the time slices is described in detail in Section 170  
 119 2.3.

120 In contrast to previously performed climate model exper- 171  
 121 iments with idealized astronomical forcing, in which obliqu- 172  
 122 uity and precession have usually been set to extreme values 173  
 123 (e.g., Tuenter et al., 2003; Mantsis et al., 2011, 2014; Erb 174  
 124 et al., 2013; Bosmans et al., 2015), our analyzes are based 175  
 125 on realistic astronomical configurations. We note that real- 176  
 126 istic and idealized forcing experiments are equally important  
 127 and complementary. Idealized experiments provide impor-

tant insight into the climate system's response to astronomi-  
 cal forcing. However, since this response may be non-linear,  
 using extreme values of astronomical parameters in ideal-  
 ized experiments may hide important aspects of astronomi-  
 cal forcing. Obviously, realistically forced experiments have  
 a stronger potential for model-data comparison.

Special focus is on the sensitivity of the West African and  
 Indian monsoon systems to obliquity and precession forcing.  
 In particular, the applicability of the global monsoon concept  
 (Trenberth et al., 2000; Wang et al., 2014) will be tested for  
 astronomical timescales.

## 2 Experimental setup

### 2.1 Model description

We use the fully coupled climate model CCSM3 with the  
 atmosphere, ocean, sea-ice and land-surface components in-  
 teractively connected by a flux coupler (Collins et al., 2006).  
 We apply the low-resolution version of the model (Yeager  
 et al., 2006) which enables us to simulate a large set of time  
 slices. In this version, the resolution of the atmosphere is  
 given by T31 spectral truncation (3.75° transform grid) with  
 26 layers, while the ocean model has a nominal horizontal  
 resolution of 3° (as has the sea-ice component) with 25 lev-  
 els in the vertical. The land model shares the same horizon-  
 tal grid with the atmosphere and includes components for  
 biogeophysics, biogeochemistry, the hydrological cycle as  
 well as a Dynamic Global Vegetation Model (DGVM) based  
 on the Lund-Potsdam-Jena (LPJ)-DGVM (Sitch et al., 2003;  
 Levis et al., 2004; Bonan and Levis, 2006). The DGVM  
 predicts the distribution of 10 plant functional types (PFT)  
 which are differentiated by physiological, morphological,  
 phenological, bioclimatic, and fire-response attributes (Levis  
 et al., 2004). In order to improve the simulation of land-  
 surface hydrology and hence the vegetation cover, new pa-  
 rameterizations for canopy interception and soil evaporation  
 were implemented into the land component (Oleson et al.,  
 2008; Handiani et al., 2013; Rachmayani et al., 2015). PFT  
 population densities are restored annually, while the land and  
 atmosphere models are integrated with a 30 minutes time  
 step.

### 2.2 Setup of experiments

To serve as a reference climatic state, a standard pre-  
 industrial (PI) control simulation was carried out follow-  
 ing PMIP (Paleoclimate Modelling Intercomparison Project)  
 guidelines with respect to the forcing (e.g., Braconnot et al.,  
 2007). The PI boundary conditions include astronomical pa-  
 rameters of 1950 AD, atmospheric trace gas concentrations  
 from the 18th century (Table 1) as well as pre-industrial dis-  
 tributions of atmospheric ozone, sulfate aerosols, and car-  
 bonaceous aerosols (Otto-Bliesner et al., 2006). The solar

constant is set to  $1365 \text{ Wm}^{-2}$ . The PI control run was inte-  
grated for 1000 years starting from modern initial conditions,  
except for the vegetation which starts from bare soil.

In total, 13 interglacial time slice experiments were carried  
out, all branching off from year 600 of the PI spin-up run and  
running for 400 years each. Note that the present study only  
focusses on the surface climate, for which this spin-up time  
should be sufficient, whereas the deep ocean usually needs  
more time to adjust to changes in forcing (Renssen et al.,  
2006).

Boundary conditions for the selected time slices which are  
spanning the last 615 kyr comprise astronomical parameters  
(Berger, 1978) and GHG concentrations as given in Table 1,  
while other forcings (ice sheet configuration, ozone distribu-  
tion, sulfate aerosols, carbonaceous aerosols, solar constant)  
were kept as in the PI control run. The mean of the last 100  
simulation years of each experiment was used for analysis.

We note that a fixed calendar based on a 365-day year is  
used for all experiments (Joussaume and Braconnot, 1997;  
Chen et al., 2011). The greatest calendar-biases are known  
to occur in boreal fall, whereas the effects in boreal summer  
and winter (the seasons discussed in the present study) are  
generally small (e.g., Timm et al., 2008).

### 2.3 Selection of interglacial time slices

For MIS 1, the mid-Holocene time slice of 6 kyrBP using  
standard PMIP forcing (Braconnot et al., 2007) was com-  
plemented by an early-Holocene 9 kyrBP simulation when  
Northern Hemisphere summer insolation was close to max-  
imum (Fig. 1). Two time slices, 125 and 115 kyrBP, were  
also chosen for the last interglacial (MIS 5e). Similar to  
9 kyrBP, the 125 kyrBP time slice is also characterized by  
nearly peak interglacial forcing, although the MIS 5 insola-  
tion forcing is stronger due to a greater eccentricity of the  
Earth's orbit. Moreover, the global benthic  $\delta^{18}\text{O}$  stack is  
at minimum around 125 kyrBP (Lisiecki and Raymo, 2005).  
By contrast, boreal summer insolation is close to minimum  
at 115 kyrBP, which marked the end of MIS 5e (Fig. 1).  
GHG concentrations for the MIS 5 time slices were taken as  
specified by PMIP-3 (Lunt et al., 2013).

For the unusually long interglacial of MIS 11 (e.g., Milker  
et al., 2013) three time slices were chosen, 394, 405, and  
416 kyrBP. The middle time slice (405 kyrBP) coincides  
with the  $\delta^{18}\text{O}$  minimum of MIS 11 (Lisiecki and Raymo,  
2005; Milker et al., 2013). The time slices of 394 and  
416 kyrBP are characterized by almost identical precession  
and similar GHG concentrations (Table 1), but opposite ex-  
tremes of obliquity (maximum at 416 kyrBP, minimum at  
394 kyrBP; Fig. 1). This allows to study the quasi-isolated  
effect of obliquity forcing (Berger, 1978) during MIS 11 by  
directly comparing the results of these two time slices. As  
opposed to idealized simulations of obliquity forcing (e.g.,  
Tuenter et al., 2003; Mantsis et al., 2011, 2014; Erb et al.,  
2013) our approach considers quasi-realistic climate states of

the past using realistic forcings. In the same vein, time slices  
for MIS 13 have been chosen. Obliquity is at maximum at  
495 kyrBP and at minimum at 516 kyrBP, while precession  
is almost identical. Unlike the 394 and 416 kyrBP time slices  
of MIS 11 which are characterized by intermediate preces-  
sion values, precession is at maximum at 495 and 516 kyrBP,  
i.e. Northern Hemisphere summer occurs at aphelion caus-  
ing weak insolation forcing (Yin et al., 2009). In addition,  
the 504 kyrBP time slice was picked because of peak North-  
ern Hemisphere summer insolation forcing, while obliquity  
has an intermediate value (Fig. 1).

Finally, two time slice experiments were performed  
for MIS 15 to assess the climatic response to minimum  
(579 kyrBP) and maximum (609 kyrBP) precession. Ac-  
cordingly, Northern Hemisphere summer insolation is near  
maximum and minimum at 579 and 609 kyrBP, respec-  
tively. In addition, a third MIS 15 experiment was carried out  
(615 kyrBP) with insolation forcing in between the two oth-  
ers (Fig. 1). Moreover, the 615 kyrBP time slice has a very  
special seasonal insolation pattern as we will see in the next  
section. All three MIS 15 time slices coincide with minimum  
 $\delta^{18}\text{O}$  values (Lisiecki and Raymo, 2005).

Table 1 summarizes the GHG forcing of all experiments  
with values based on Lüthi et al. (2008), Louergue et al.  
(2008), and Schilt et al. (2010) using the EPICA Dome C  
timescale EDC3, except for the MIS 1 and MIS 5 experi-  
ments, where GHG values were chosen following the PMIP  
guidelines (see above). We note that due to the uneven distri-  
bution of methane sources and sinks over the latitudes, val-  
ues of atmospheric  $\text{CH}_4$  concentration derived from Antarc-  
tic ice cores present a lower estimate of global  $\text{CH}_4$  con-  
centration. We further note that some results from the MIS  
1 (6 and 9 kyrBP), MIS 5 (125 kyrBP), and MIS 11 (394,  
405, and 416 kyrBP) experiments were previously published  
(Lunt et al., 2013; Milker et al., 2013; Kleinen et al., 2014;  
Rachmayani et al., 2015).

### 2.4 Insolation anomalies

Annual cycles of the latitudinal distribution of insolation at  
the top of the atmosphere (as anomalies relative to PI) are  
shown in Fig. 2 for each experiment. The insolation pat-  
terns can be divided into three groups which differ in their  
seasonal distribution of incoming energy. Group I is charac-  
terized by high Northern Hemisphere summer insolation as  
exhibited for the 6 and 9 kyrBP (MIS 1), 125 kyrBP (MIS  
5), 405 and 416 kyrBP (MIS 11), 504 kyrBP (MIS 13), and  
579 kyrBP (MIS 15) time slices. In most (but not all, see be-  
low) cases this is due to an astronomical configuration with  
northern summer solstice at or close to perihelion. Group II  
comprises anomalies with low boreal summer insolation as  
shown for 115 kyrBP (MIS 5), 495 and 516 kyrBP (MIS 13),  
and 609 kyrBP (MIS 15). In these cases, northern winter sol-  
stice is near perihelion. Group III is characterized by changes  
in the sign of the Northern Hemisphere insolation anoma-

Stage	Time slice (ka BP)	CO <sub>2</sub> (ppmv)	CH <sub>4</sub> (ppbv)	N <sub>2</sub> O (ppbv)
MIS 1	0	280	760	270
	6	280	650	270
	9	265	680	260
MIS 5	115	273	472	251
	125	276	640	263
MIS 11	394	275	550	275
	405	280	660	285
	416	275	620	270
MIS 13	495	240	487	249
	504	240	525	278
	516	250	500	285
MIS 15	579	252	618	266
	609	259	583	274
	615	253	617	274

**Table 1.** Atmospheric GHG concentrations used in the interglacial experiments.

lies from spring to summer and consists of two dates (394 and 615 kyrBP). At 394 (615 kyrBP) the insolation anomaly spring-to-summer change is from positive (negative) to negative (positive). In these cases, spring equinox (394 kyrBP) or fall equinox (615 kyrBP) are close to perihelion.

### 3 Results

#### 3.1 JJAS surface temperature anomalies

The response of boreal summer (June–July–August–September, JJAS) surface temperature to the combined effect of insolation and GHG in all individual climates (Fig. 3) shows warm conditions (relative to PI) over most parts of the continents in Group I (6, 9, 125, 405, 416, 504, and 579 kyrBP) with the three warmest anomalies at 9, 125, and 579 kyrBP. The warm surface conditions can largely be explained by the immediate effect of high summer insolation and a reduction of the Northern Hemisphere sea-ice area by about 15–20% (not shown) relative to PI. The large thermal capacity of the ocean explains a larger temperature response over land than over the ocean (Herold et al., 2012; Nikolova et al., 2013). Simulated cooling over North Africa (10–25° N) and India in the Group I experiments is caused by enhanced monsoonal rainfall in these regions, which is associated with increased cloud cover, i.e. reduced short-wave fluxes, and enhanced land surface evapotranspiration, i.e. greater latent cooling (e.g., Braconnot et al., 2002, 2004; Zheng and Braconnot, 2013). Cooling in some parts of the Southern Ocean in most Group I experiments is likely attributable to an austral summer remnant effect of local insolation (see below) as in Yin and Berger (2012). The 416 kyrBP time slice, however, differs from the other Group I members by anomalously cold conditions over the Southern Hemisphere continents. Again, this behaviour can be explained by the immediate effect of the insolation, which shows negative anomalies in the Southern Hemisphere during the JJAS

season (Fig. 2). As such, the 416 kyrBP time slice must be considered a special case in Group I. While high Northern Hemisphere summer insolation is related to low precession in most Group I members, positive anomalies of Northern Hemisphere summer insolation at 416 kyrBP are attributable to a maximum in obliquity (Fig. 1), yielding the Northern-versus-Southern Hemisphere insolation contrast.

In contrast to Group I, Group II climates exhibit anomalously cold JJAS surface temperatures globally with the three coldest anomalies at 115, 516, and 609 kyrBP. Again, the temperature response can largely be explained by the direct response to insolation forcing, amplified in high latitudes by an increase of the sea-ice cover (about 5% in the Arctic compared to PI). Due to a particular combination of high precession and eccentricity with low obliquity the insolation forcing and surface temperature response is strongest for the 115 kyrBP time slice. Group II warming in the North African and Indian monsoon regions is associated with increased aridity and reduced cloudiness.

Group III climates (394 and 615 kyrBP) show rather complex temperature anomaly patterns, especially in the tropics. In the 394 kyrBP time slice, however, northern continental regions show a distinct cooling, whereas continental regions exhibit an overall warming in the Southern Hemisphere (except for Antarctica). To a large extent, the 394 kyrBP time slice shows a reversed JJAS temperature anomaly pattern compared to the 416 kyrBP simulation over the continental regions, except for Antarctica.

#### 3.2 DJF surface temperature anomalies

Boreal winter (December–January–February, DJF) surface temperature anomalies are presented in Fig. 4. Generally low DJF insolation in Group I time slices (Fig. 2) results in anomalously cold surface conditions over most of the globe, particularly strong in the 579 kyrBP (MIS 15) time slice. However, anomalously warm conditions in the Arctic stand

in contrast to the global DJF cooling at 6, 9, 125, 405, and 416 kyrBP. The Arctic warming is due to the remnant effect of the polar summer insolation through ocean–sea ice feedbacks (Fischer and Jungclauss, 2010; Herold et al., 2012; Yin and Berger, 2012; Kleinen et al., 2014). Anomalous short-wave radiation during the Arctic summer leads to enhanced melting of sea ice and warming of the upper polar ocean. The additional heat received by the upper ocean delays the formation of winter sea ice, reduces its thickness and finally leads to a warming of the winter surface atmospheric layer by enhanced ocean heat release (Yin and Berger, 2012). Arctic winter warming is not present in the 504 kyrBP (MIS 13) and 579 kyrBP (MIS 15) time slices in Group I, where the summer remnant effect in the Arctic is probably masked by a global cooling that is induced by low GHG concentrations typical for early Brunhes (MIS 13 and before) interglacials.

To a large extent, DJF surface temperature anomaly patterns are reversed in Group II with warming over most continental regions. Moreover, the summer remnant effect reverses to a substantial cooling in the Arctic region. Temperature anomaly patterns in Group III are, again, rather complex. Interestingly, most Northern Hemisphere continental regions remain relatively cold during boreal winter (as in summer) in the 394 kyrBP simulation. Relatively low GHG concentrations, especially  $\text{CH}_4$ , contribute to the year-round extratropical cooling in this time slice.

### 3.3 JJAS precipitation anomalies

Boreal summer precipitation shown in Fig. 5 exhibits intensified rainfall in the monsoon belt from North Africa to India, via the Arabian Peninsula, in all Group I simulations in response to high summer insolation (Prell and Kutzbach, 1987; de Noblet et al., 1996; Tuenter et al., 2003; Braconnot et al., 2007). By contrast, the same monsoon regions experience anomalously dry conditions in the Group II (low boreal summer insolation) experiments. The most interesting results regarding the tropical rainfall response to astronomical forcing appear in Group III, where the monsoonal precipitation anomalies show opposite signs in North Africa (Sahel region) and India.

Table 2 summarizes the summer monsoonal rainfall amounts for the North African ( $20^\circ\text{W}$ – $30^\circ\text{E}$ ;  $10$ – $25^\circ\text{N}$ ) and Indian ( $70$ – $100^\circ\text{E}$ ;  $10$ – $30^\circ\text{N}$ ) regions. Highest rainfall in the North African monsoon region occurs in the 9, 125, 504, and 579 kyrBP time slice runs (all Group I) associated with low precession values (Fig. 1). Driest conditions occur at 115, 495, 516, and 609 kyrBP (all Group II) associated with precession maxima (Fig. 1). As in North Africa, Group I (Group II) experiments exhibit anomalously wet (dry) monsoon conditions in India.

### 3.4 Net Primary Production (NPP) anomalies

Vegetation responds to changes in surface temperature and precipitation and, in certain regions, may feedback to the climate (cf. Rachmayani et al., 2015). Figure 6 shows the simulated changes in NPP, reflecting increase/decrease and expansion/retreat of vegetation covers, relative to PI. In high Arctic latitudes, NPP increases in the Group I simulations, except for 405 kyrBP where temperature changes are probably too small to substantially affect the vegetation. By contrast, Arctic NPP declines in the Group II experiments, albeit only in the easternmost part of Siberia in the 495 kyrBP experiment. A substantial decline of Arctic NPP is also simulated for 394 kyrBP (Group III). In the tropical regions, vegetation changes are mostly governed by precipitation. Consequently, enhanced rainfall results in increased NPP over North Africa, the Arabian Peninsula and India in all Group I experiments. In North Africa increased NPP is associated with a northward shift of the Sahel–Sahara boundary. The largest shifts are simulated for 125 and 579 kyrBP in accordance with maximum North African rainfall anomalies. In these experiments, a complete greening of the Arabian Desert is simulated. Opposite NPP anomalies in the tropical monsoon regions are simulated in the Group II experiments. In Group III, NPP increases result from anomalously high rainfall in North Africa (615 kyrBP) or India (394 kyrBP).

### 3.5 Climatic effects of obliquity variations during MIS 11 and MIS 13

The MIS 11 time slices 394 and 416 kyrBP show opposite obliquity extremes (at similar precession), as do the MIS 13 time slices 495 and 516 kyrBP (Fig. 1). Insolation differences between the high obliquity (416, 495 kyrBP) and low obliquity (394, 516 kyrBP) cases (i.e. 416 minus 394 and 495 minus 516 kyrBP) are displayed in Fig. 7. The effect of high obliquity is to strengthen the seasonal insolation cycle. At low latitudes, the effect of obliquity on insolation is small.

For the maximum obliquity time slices (416 and 495 kyrBP) relatively high boreal summer insolation directly translates into positive surface temperature anomalies over Northern Hemisphere continents, except for the low latitudes where reduced local insolation (especially in the MIS 13 case) and higher monsoon rainfall (especially in the MIS 11 case, see below) lead to surface cooling (Fig. 8a,b). By contrast, receiving anomalously low insolation during austral winter, Southern Hemisphere continents exhibit anomalously cold surface temperatures. For the 416–394 kyrBP case, however, the Antarctic continent and the Southern Ocean show large-scale warming during the JJAS season, which can be attributed to a south polar summer remnant effect as the austral summer insolation anomaly is extremely high in this experiment (Fig. 7a). Higher GHG concentrations at 416 compared to 394 kyrBP may add to this warming. Owing to a smaller south polar summer insolation anomaly (Fig. 7)

Stage	Time slice	North Africa (mm day <sup>-1</sup> )	North Africa Anomaly (mm day <sup>-1</sup> )	India (mm day <sup>-1</sup> )	India Anomaly (mm day <sup>-1</sup> )
MIS 1	0 ka	2.44±0.04		6.59±0.12	
	6 ka	3.41±0.04	0.97	6.91±0.10	0.32
	9 ka	3.71±0.04	1.27	7.36±0.08	0.77
MIS 5	115 ka	1.59±0.02	-0.85	5.90±0.15	-0.69
	125 ka	3.79±0.04	1.35	7.26±0.07	0.67
MIS 11	394 ka	2.37±0.04	-0.07	6.92±0.12	0.33
	405 ka	3.20±0.04	0.76	6.95±0.11	0.36
	416 ka	3.06±0.04	0.62	7.13±0.12	0.54
MIS 13	495 ka	1.91±0.04	-0.53	6.11±0.13	-0.48
	504 ka	3.72±0.04	1.28	7.11±0.08	0.52
	516 ka	1.88±0.04	-0.56	6.22±0.13	-0.37
MIS 15	579 ka	3.77±0.04	1.33	7.72±0.07	1.13
	609 ka	1.49±0.02	-0.95	6.10±0.13	-0.49
	615 ka	3.21±0.04	0.77	6.27±0.13	-0.32

**Table 2.** Summer (JJAS) precipitation over North Africa (20° W–30° E and 10° N–25° N) and over India (70° E–100° E and 10° N–30° N) along with anomalies relative to PI. Absolute precipitation values are given with standard error ( $2\sigma$ ) based on 100 simulation years of each experiment.

the summer remnant effect is smaller in the 495–516 kyrBP case and even surpassed by anomalously low GHG forcing in the 495 kyrBP time slice, leading to negative austral winter temperature anomalies in the Southern Ocean and Antarctica (Fig. 7b).

During boreal winter, Northern Hemisphere continents show large-scale cooling in response to high obliquity (and hence relatively low insolation), except for the Arctic realm where the summer remnant effect results in substantial positive surface temperature anomalies (Fig. 8c and d). During the same season (DJF) anomalously high insolation causes surface warming in the Southern Hemisphere in response to high obliquity. As a general pattern in the annual mean, maximum-minus-minimum obliquity forcing causes anomalous surface warming at high latitudes and surface cooling at low latitudes caused by seasonal and annual insolation anomalies in combination with climate feedbacks like the polar summer remnant effect and monsoon rainfall.

Despite the weak insolation signal at low latitudes, substantial obliquity-induced changes in tropical precipitation are simulated (Fig. 8e and f). The strongest signal is found in the North African monsoon region in the MIS 11 experiments, where greater JJAS precipitation occurs during maximum obliquity at 416 kyrBP than during the obliquity minimum at 394 kyrBP. A positive Sahel rainfall anomaly is also found in the MIS 13 experiments (495–516 kyrBP), but much weaker than in the MIS 11 case (416–394 kyrBP). We suppose that the obliquity-induced increase in North African monsoonal rainfall is counteracted by the high precession at 495 kyrBP that tends to weaken the monsoon. Considering the spatiotemporal insolation patterns (Fig. 7) the Northern Hemisphere tropical summer insolation anomaly is less negative and the meridional summer insolation gradient anomalies are generally greater in the 416–394 kyrBP case compared to the 495–516 kyrBP case. Both features of the insolation anomaly favor a strong North African monsoon (see Discussion).

3.6 Evaluating the climatic effects of astronomical and GHG forcings through correlation maps

### 3.6 Evaluating the climatic effects of astronomical and GHG forcings through correlation maps

In order to evaluate the climatic effects of obliquity, precession and GHG concentrations, linear correlations between the individual forcing parameters and climatic fields (surface temperature, precipitation) were calculated from the 14 time slice experiments (13 interglacial time slices plus PI). To this end, each climate variable (temperature, precipitation) was averaged over the last 100 years of each experiment. Linear correlation coefficients were calculated at each grid point. Significance of correlations was tested by a two-sided Student's t test with 95% confidence level. Total radiative forcing from CO<sub>2</sub>, CH<sub>4</sub>, and N<sub>2</sub>O in each experiment was calculated based on a simplified expression (IPCC, 2001).

Figure 9 shows the corresponding correlation maps for annual mean, boreal summer, and boreal winter surface temperature. As expected, GHG forcing is positively correlated with surface temperature over most regions of the globe (Fig. 9a), which is particularly pronounced in the annual mean. For the seasonal correlation maps (boreal summer and winter) the correlation coefficients are smaller because of the dominant impact of obliquity and precession forcing.

As already described in the previous subsection, the general surface temperature pattern of high obliquity forcing is warming at high latitudes and cooling at low latitudes (Fig. 9b). High precession (northern solstice near aphelion) leads to boreal summer surface cooling over most extratropical regions (Fig. 9c). However, surface warming occurs in some tropical regions as a response to weaker monsoons. During boreal winter, anomalously high insolation causes anomalous surface warming except in the Arctic (due to the summer

remnant effect) and northern Australia (due to a stronger regional monsoon).

Correlation maps for annual mean, boreal summer, and boreal winter precipitation are shown in Fig. 10. GHG radiative forcing exhibits no clear response in precipitation except for the high latitudes where the hydrologic cycle accelerates with higher GHG concentrations (Fig. 10a). Since the GHG variations are relatively small, the effects of astronomical forcing on the monsoons are way larger than the effects of GHG variations during the interglacials. Arctic precipitation is also amplified by high obliquity during summer (Fig. 10b). Obliquity also strengthens the monsoonal rainfall in North Africa (Sahel region), whereas no effect of obliquity can be detected for the Australian monsoon. The sensitivity of other monsoon systems to obliquity changes is also weak or even absent in our experiments. The most robust response of the hydrologic cycle is found for precession (Fig. 10c). In particular, high precession reduces summer rainfall in the monsoon belt from North Africa to India as well as in the Arctic realm. East Asian rainfall shows a somewhat heterogeneous pattern and is, in general, only weakly coupled with the Indian and African monsoons. This finding is consistent with a recent model intercomparison study by Dallmeyer et al. (2015). During boreal winter, the hydrologic cycle strengthens in the Arctic and Antarctic regions, while Southern Hemisphere monsoon systems amplify resulting in enhanced rainfall over South America, southern Africa, and northern Australia in response to high precession. We note that these monsoonal rainfall changes go along with distinct surface temperature signals in the annual mean (Fig. 9c).

#### 4 Discussion

While most time slices presented in this study were simulated for the first time using a comprehensive CGCM, the 6, 115 and 125 kyrBP time slices have been studied extensively in previous model studies. In general, the CCSM3 results are in line with these previous studies in terms of large-scale temperature and precipitation patterns. Warm boreal summer conditions (relative to PI) over most parts of the continents and the Arctic are a general feature in paleoclimatic simulations of the mid-Holocene (6 kyrBP), while the North African and South Asian monsoon regions are anomalously cold due to enhanced rainfall (Braconnot et al., 2007). Though evidenced by proxy records (e.g., McClure, 1976; Hoelzmann et al., 1998; Fleitmann et al., 2003), several models fail to simulate wetter mid-Holocene conditions over the Arabian Peninsula (cf. <https://pmip3.lscce.fr/database/maps/>), while CCSM3 simulates not only enhanced rainfall but also greening of the Arabian Desert. The 125 kyrBP surface temperature pattern shows similar features than the 6 kyrBP pattern, but much more pronounced due to the larger eccentricity and hence stronger precessional forcing. However, compared to other simulations of the

last interglaciation, our CCSM3 simulation produces a relatively cold MIS 5e surface climate as shown by Lunt et al. (2013). At 115 kyrBP, surface temperature anomalies show the opposite sign with dramatic cooling over the Arctic and the northern continental regions providing ideal conditions for glacial inception (e.g., Khodri et al., 2005; Kaspar and Cubasch, 2007; Jochum et al., 2012). A retreat of the vegetation at high northern latitudes tends to amplify the insolation-induced cooling (cf. Gallimore and Kutzbach, 1996; Meissner et al., 2003).

A recent simulation of the MIS 13 time slice at 506 kyrBP using the CGCM HadCM3 (Muri et al., 2013) can be compared to our 504 kyrBP time slice using CCSM3. Global patterns of surface temperature anomalies (relative to PI) are remarkably similar in the two different simulations with warm anomalies over all continents (except for the North African and South Asian monsoon regions) in boreal summer and worldwide cold anomalies during boreal winter. Moreover, both simulations show anomalously high boreal summer precipitation over northern South America, North and central Africa as well as the South Asian monsoon region.

Although our CCSM3 results show general agreement with other model studies, the validation of model results with data is usually not straightforward. The reader is referred to previous work where our CCSM3 simulation of 125 kyrBP (Lunt et al., 2013) as well as the MIS 11 simulations have been extensively compared to proxy data (Milker et al., 2013; Kleinen et al., 2014). Taken together, these and other studies (e.g., Lohmann et al., 2013) indicate that CGCMs tend to produce generally smaller interglacial temperature anomalies than suggested by the proxy records. So far, the reason for these discrepancies is unsolved (cf. Liu et al., 2014), but Hessler et al. (2014) pointed out that uncertainties associated with sea surface temperature reconstructions are generally larger than interglacial temperature anomalies. Thus, currently available surface temperature proxy data cannot serve as a target for benchmarking interglacial model simulations.

Two time slices of MIS 11 (394 vs. 416 kyrBP) and two time slices of MIS 13 (495 vs. 516 kyrBP) allow the investigation of (almost pure) obliquity effects on global climate, although the GHG and precession are not exactly the same between the time slices. As such, the results from these simulations can be compared to previously performed idealized model experiments in which obliquity has been changed from maximum to minimum values (Tuenter et al., 2003; Mantsis et al., 2011; Erb et al., 2013; Bosmans et al., 2015). The common results of those idealized and our experiments can be summarized as follows. High-versus-low obliquity climates are characterized by strong warming over the Northern Hemisphere extratropics and slight cooling in the tropics during boreal summer. During boreal winter, a moderate cooling over large portions of the Northern Hemisphere continents and a strong warming at high southern latitudes is found. The obliquity-induced Northern Hemisphere summer warming appears to be of particular interest for the MIS 13

climate evolution. At 495 kyrBP, precession is at maximum, but the global benthic  $\delta^{18}\text{O}$  stack by Lisiecki and Raymo (2005) does not show the expected increase towards heavier values which would indicate colder conditions and Northern Hemisphere cryosphere expansion (Fig. 1). In fact, despite high precession, the 495 kyrBP simulation exhibits the warmest Northern Hemisphere summer temperatures from all Group II experiments (Fig. 3), which can be attributed to concomitant high obliquity. We therefore hypothesize that the Northern Hemisphere summer climate at 495 kyrBP was not cold enough for ice sheets to grow and global ocean  $\delta^{18}\text{O}$  to increase. We note, however, that the benthic  $\delta^{18}\text{O}$  stack is subject to age model uncertainties of a few thousand years.

Moreover, our CCSM3 results as well as the studies by Tuentner et al. (2003) and Bosmans et al. (2015) suggest a significant effect of obliquity on West African monsoon rainfall despite the weak insolation signal at low latitudes. Bosmans et al. (2015) have shown that obliquity-induced changes in moisture transport towards North Africa result from changes in the meridional insolation gradient (Davis and Brewer, 2009). However, the impact of obliquity on the monsoon also depends on precession. In the 495–516 kyrBP experiment the obliquity-effect on the West African monsoon is minor, as both time slices (495 and 516 kyrBP) are characterized by precession maxima leading to extremely weak monsoonal circulation and rainfall in both cases. The existence of a  $\sim 41$  kyr cyclicity (in addition to astronomical-related  $\sim 100$  and 19–23 kyr cycles) in reconstructions of North African aridity during the Quaternary has usually been attributed to obliquity-forced Northern Hemisphere cryosphere effects on the monsoon climate (e.g., Bloemendal and deMenocal, 1989; deMenocal et al., 1993; Tiedemann et al., 1994; deMenocal, 1995; Kroon et al., 1998). Our model results along with the studies by Tuentner et al. (2003) and Bosmans et al. (2015) complement this picture, showing that the direct insolation-gradient forcing associated with obliquity can contribute to West African monsoon changes without involving high-latitude remote climate forcing associated with Northern Hemisphere ice sheets.

According to the CCSM3 results, the Indian monsoon is less sensitive to direct obliquity (insolation gradient) forcing than the West African monsoon. This finding is consistent with proxy records from the Arabian Sea that show substantial 41 kyr (obliquity) periodicity only after the onset of Quaternary glacial cycles when waxing and waning of northern ice sheets could have worked as an agent for the transfer of obliquity forcing to the Indian monsoon region (Bloemendal and deMenocal, 1989). In general, it is found that the two monsoon systems do not always vary in concert. This is particularly evident in the Group III experiments (394 and 615 kyrBP) where the precipitation anomalies over North Africa and India have opposite signs (Table 2). Considering the annual insolation maps of the 394 and 615 kyr experiments (Fig. 2), West African monsoon rainfall turns out to be most sensitive to changes in summer insolation, whereas

spring/early summer insolation is more important for monsoon rainfall over India. Similar results have been found by Braconnot et al. (2008). It has been argued that the reason is a resonant response of the Indian monsoon to the insolation forcing when maximum insolation anomalies occur near the summer solstice and a resonant response of the African monsoon – which has its rainfall maximum one month later in the annual cycle than the Indian monsoon – when the maximum insolation change is delayed after the summer solstice. The different responses to specific forcings and the sometimes out-of-phase behaviour of the African and Indian monsoon systems challenge the global monsoon concept – according to which all regional monsoon systems are part of one seasonally varying global-scale atmospheric overturning circulation in the tropics (Trenberth et al., 2000; Wang et al., 2014) – at astronomical timescales.

Another important result of our study is associated with obliquity forcing of high-latitude precipitation anomalies. As obliquity increases, high latitudes become warmer and the gradient in solar heating between high and low latitudes decreases, while precipitation over high-latitude continental regions increases (Fig. 10b). This result clearly contradicts the “gradient hypothesis” by Raymo and Nisancioglu (2003) according to which low obliquity would favour polar ice-sheet growth through enhanced delivery of moisture owing to an increased meridional solar heating gradient.

Since  $\text{CO}_2$  and other GHG variations are relatively small during the interglacials, the effects of astronomical forcing on the monsoons are substantially larger. Hence, GHG forcing shows a clear response in precipitation only for the high latitudes where the hydrologic cycle accelerates with higher GHG concentrations. In the monsoon regions, interglacial rainfall variations are almost entirely controlled by astronomical forcing.

The use of a modern ice-sheet configuration for all interglacial time slice experiments, however, must be considered a limitation of the present study. Future studies should include the effects of changing ice sheets and associated meltwater fluxes in shaping interglacial climates. Large Northern Hemisphere ice sheets might have played an important role for regional and global climates especially during early Brunhes interglacials (MIS 13 and before) as suggested by, e.g., Yin et al. (2008) and Muri et al. (2013). But also during late Brunhes interglacial stages, like the Holocene, model studies suggest an influence of changing land ice on the interglacial climate evolution (Renssen et al., 2009; Marzin et al., 2013). The tremendous uncertainties regarding ice-sheet reconstructions beyond the present interglacial could be taken into account by performing sensitivity experiments.

## 5 Conclusions

Using CCSM3-DGVM, 13 interglacial time slice experiments were carried out to study global climate variability

735 between and within Quaternary interglacials. The selec- 790  
736 tion of interglacial time slices was based on different aspects 791  
737 of inter- and intra-interglacial variability and associated as- 792  
738 tronomical forcing. As such, our approach is complemen- 793  
739 tary to both idealized astronomical forcing experiments (e.g., 794  
740 Tuenter et al., 2003; Mantsis et al., 2011, 2014; Erb et al., 795  
741 2013; Bosmans et al., 2015) and climate simulations that fo- 796  
742 cussed on peak interglacial forcing (Herold et al., 2012; Yin 797  
743 and Berger, 2012).

744 In this study, the different roles of obliquity, precession 798  
745 and GHG forcing on surface temperature and precipitation 799  
746 patterns have been disentangled. In most regions seasonal 800  
747 surface temperature anomalies could largely be explained by 801  
748 local insolation anomalies induced by the astronomical forc- 802  
749 ing. Climate feedbacks modify the surface temperature re- 803  
750 sponse in specific regions, particularly in the monsoon do- 804  
751 mains and the polar oceans. GHG forcing may also play a 805  
752 role for seasonal temperature anomalies, especially in high  
753 latitudes and the early Brunhes interglacials MIS 13 and 15 806  
754 when GHG concentrations were much lower than during the  
755 later interglacials. 807

756 A significant role of obliquity in forcing the West African 808  
757 monsoon was found, whereas the Indian monsoon – as well 809  
758 as the other regional monsoon systems – appear to be less 810  
759 sensitive (or not sensitive at all) to obliquity changes during 811  
760 interglacials. Despite this important role of obliquity in West 812  
761 African monsoon variability, the response to precession is 813  
762 still stronger. Different responses to specific forcings and the 814  
763 obvious anti-phase behaviour of the African and Indian mon- 815  
764 soon systems in the 394 and 615 kyrBP experiments, where 816  
765 the North African rainfall anomaly has opposite sign com- 817  
766 pared to the Indian anomaly, clearly point to the fact that the 818  
767 two regional monsoon systems do not always vary in concert 819  
768 and challenge the global monsoon concept at the astronomi- 820  
769 cal timescale. 821

770 As a general pattern in the annual mean, maximum-minus- 823  
771 minimum obliquity forcing causes anomalous surface warm- 824  
772 ing at high latitudes and surface cooling at low latitudes 825  
773 caused by seasonal and annual insolation anomalies in com- 826  
774 bination with climate feedbacks like the polar summer rem- 827  
775 nant effect and monsoon rainfall. High obliquity may also 828  
776 explain relatively warm Northern Hemisphere high-latitude 829  
777 summer temperatures despite maximum precession around 830  
778 495 kyrBP (MIS 13). We hypothesize that this obliquity- 831  
779 induced high-latitude warming may have prevented a glacial 832  
780 inception at that time. Moreover, our results suggest high- 833  
781 latitude precipitation increase with increasing obliquity, con- 834  
782 tradicting the “gradient hypothesis” by (Raymo and Nisan- 835  
783 cioglu, 2003) according to which low obliquity would favour 836  
784 polar ice-sheet growth through enhanced delivery of mois- 837  
785 ture owing to an increased meridional solar heating gradient. 838

786 Future studies should include the effects of changing ice 841  
787 sheets and associated meltwater fluxes in shaping interglacial 842  
788 climates. With increasing computer power long-term tran- 843  
789 sient simulations of interglacial climates will become more 844

common. So far, transient CGCM simulations have been per-  
formed for the present (e.g., Lorenz and Lohmann, 2004;  
Varma et al., 2012; Liu et al., 2014) and the last interglacial  
(e.g., Bakker et al., 2013; Govin et al., 2014). More tran-  
sient simulations of earlier interglacials, ideally with coupled  
interactive ice-sheet models, will help to develop a signifi-  
cantly deeper understanding of interglacial climate dynam-  
ics.

**Acknowledgements.** The study was funded by the Deutsche  
Forschungsgemeinschaft (DFG) through the Priority Programme  
INTERDYNAMIC. CCSM3 simulations were performed on the  
SGI Altix supercomputer of the Norddeutscher Verbund für  
Hoch- und Höchstleistungsrechnen (HLRN). The article process-  
ing charges for this open-access publication were covered by the  
University of Bremen. We would like to thank the two anonymous  
reviewers for their constructive suggestions and helpful comments.

## References

- Bakker, P., Stone, E. J., Charbit, S., Gröger, M., Krebs-Kanzow, U.,  
Ritz, S. P., Varma, V., Khon, V., Lunt, D. J., Mikolajewicz, U.,  
Prange, M., Renssen, H., Schneider, B., and Schulz, M.: Last  
interglacial temperature evolution – a model inter-comparison,  
*Clim. Past*, 9, 605–619, doi:10.5194/cp-9-605-2013, 2013.
- Berger, A.: Long-term variations of daily insolation and Quaternary  
Climatic Changes, *J. Atmos. Sci.*, 35, 2362–2367, 1978.
- Bloemendal, J. and deMenocal, P.: Evidence for a change in the pe-  
riodicity of tropical climate cycles at 2.4 Myr from whole-core  
magnetic susceptibility measurements, *Nature*, 342, 897–900,  
1989.
- Bonan, G. B. and Levis, S.: Evaluating aspects of the Community  
Land and Atmosphere Models (CLM3 and CAM) using a dy-  
namic global vegetation model, *J. Climate*, 19, 2290–2301, 2006.
- Bosmans, J. H. C., Drijfhout, S. S., Tuenter, E., Hilgen, F. J., and  
Lourens, L. J.: Response of the North African summer monsoon  
to precession and obliquity forcings in the EC-Earth GCM, *Clim.  
Dyn.*, 44, 279–297, doi:s00382-014-2260-z, 2015.
- Braconnot, P., Loutre, M. F., Dong, B., Joussaume, S., and  
Valdes, P.: How the simulated change in monsoon at 6 kaBP is  
related to the simulation of the modern climate: results from the  
Paleoclimate Modeling Intercomparison Project, *Clim. Dyn.*, 19,  
107–121, 2002.
- Braconnot, P., Harrison, S., Joussaume, J., Hewitt, C., Kitoh, A.,  
Kutzbach, J., Liu, Z., Otto-Bleisner, B. L., Syktus, J., and We-  
ber, S. L.: Evaluation of coupled ocean-atmosphere simulations  
of the mid-Holocene, in: *Past Climate Variability Through Eu-  
rope and Africa*, edited by: Battarbee, R. W., Gasse, F., and  
Stickley, C. E., Kluwer Academic Publisher, 515–533, Dor-  
drecht, 2004.
- Braconnot, P., Otto-Bliesner, B., Harrison, S., Joussaume, S., Pe-  
terchmitt, J.-Y., Abe-Ouchi, A., Crucifix, M., Driesschaert, E.,  
Fichefet, Th., Hewitt, C. D., Kageyama, M., Kitoh, A., Laîné, A.,  
Loutre, M.-F., Marti, O., Merkel, U., Ramstein, G., Valdes, P.,  
Weber, S. L., Yu, Y., and Zhao, Y.: Results of PMIP2 coupled  
simulations of the Mid-Holocene and Last Glacial Maximum –  
Part 1: experiments and large-scale features, *Clim. Past*, 3, 261–  
277, doi:10.5194/cp-3-261-2007, 2007.



- 845 Braconnot, P., Marzin, C., Grnégroire, L., Mosquet, E., and Marti, 904  
 846 O.: Monsoon response to changes in Earth's orbital parame- 905  
 847 ters: comparisons between simulations of the Eemian and of the 906  
 848 Holocene, *Clim. Past*, 4, 281–294, doi:10.5194/cp-4-281-2008, 907  
 849 2008. 908
- 850 Chen, G.S., Kutzbach, J.E., Gallimore, R., Liu, Z.: Calen- 909  
 851 dar effect on phase study in paleoclimate transient simula- 910  
 852 tion with orbital forcing, *Climate Dyn.*, 37.9–10: 1949–1960, 911  
 853 doi:10.1007/s00382-010-0944-6, 2011. 912
- 854 Collins, W. D., Bitz, C. M., Blackmon, M. L., Bonan, G. B., 913  
 855 Bretherton, C. S., Carton, J. A., Chang, P., Doney, S. C., 914  
 856 Hack, J. J., Henderson, T. B., Kiehl, J. T., Large, W. G., 915  
 857 McKenna, D. S., Santer, B. D., and Smith, R. D.: The Com- 916  
 858 munity Climate System Model version 3 (CCSM3), *J. Climate*, 917  
 859 19, 2122–2143, doi: 110.1175/JCLI3761.1, 2006. 918
- 860 Crucifix, M., Loutre, F. M.: Transient simulations over the last inter- 919  
 861 glacial period (126–115 kyr BP): feedback and forcing analysis, 920  
 862 *Clim. Dyn.*, 19, 417–433, 2002. 921
- 863 Dallmeyer, A., Claussen, M., Fischer, N., Haberkorn, K., Wagner, 922  
 864 S., Pfeiffer, M., Jin, L., Khon, V., Wang, Y., and Herzsuh, 923  
 865 U.: The evolution of sub-monsoon systems in the Afro-Asian 924  
 866 monsoon region during the Holocene comparison of different 925  
 867 transient climate model simulations, *Clim. Past*, 11, 305–326, 926  
 868 doi:10.5194/cp-11-305-2015, 2015. 927
- 869 Davis, B. A. S. and Brewer, S.: astronomical forcing and role 928  
 870 of the Latitudinal Insolation/Temperature Gradient, *Clim. Dyn.*, 929  
 871 32, 143–165, doi: http://dx.doi.org/10.1007/s00382-008-0480- 930  
 872 910.1007/s00382-008-0480-9, 2009. 931
- 873 deMenocal, P. B., Ruddiman, W. F., and Pokras, E. K.: In- 932  
 874 fluences of high- and low-latitude processes on African cli- 933  
 875 mate: Pleistocene eolian records from equatorial Atlantic Ocean 934  
 876 Drilling Program Site 663, *Paleoceanography*, 8, 209–242, 935  
 877 doi:10.1029/93PA02688, 1993. 936
- 878 deMenocal, P. B.: Plio-Pleistocene African climate, *Science*, 270, 937  
 879 53–59, doi:10.1126/science.270.5233.53, 1995. 938
- 880 de Noblet, N., Braconnot, P., Joussaume, S., and Masson, V.: Sensi- 939  
 881 tivity of simulated Asian and African boreal summer monsoons 940  
 882 to astronomically induced variations in insolation 126, 115 and 941  
 883 6 kBP, *Clim. Dyn.*, 12, 589–603, 1996. 942
- 884 Dutton, A. and Lambeck, K.: Ice Volume and Sea Level During the 943  
 885 Last Interglacial, *Science*, 337, 216–219, 2012. 944
- 886 Dutton, A., Carlson, A. E., Long, A. J., Milne, G. A., Clark, P. 945  
 887 U., DeConto, R., Horton, B. P., Rahmstorf, S., Raymo, M. E.: 946  
 888 Sea-level rise due to polar ice-sheet mass loss during past warm 947  
 889 periods, *Science*, 349, doi: 10.1126/science.aaa4019, 2015. 948
- 890 Erb, M. P., Broccoli, A. J., and Clement, A. C.: The contribution of 949  
 891 radiative feedbacks to astronomically driven climate change, *J.* 950  
 892 *Climate*, 26, 5897–5914, 2013. 951
- 893 Fischer, N. and Jungclaus, J. H.: Effects of astronomical forcing on 952  
 894 atmosphere and ocean heat transports in Holocene and Eemian 953  
 895 climate simulations with a comprehensive Earth system model, 954  
 896 *Clim. Past*, 6, 155–168, doi: 10.5194/cp-6-155-2010, 2010. 955
- 897 Fleitmann, D., Burns, S. J., Mudelsee, M., Neff, U., Kramers, J., 956  
 898 Mangini, A., and Matter, A.: Holocene forcing of the Indian 957  
 899 monsoon recorded in a stalagmite from Southern Oman, *Science*, 958  
 900 300, 1737–1739, 2003. 959
- 901 Gallimore, R. G. and Kutzbach, J. E.: Role of astronomically in- 960  
 902 duced changes in tundra area in the onset of glaciation, *Nature*, 961  
 903 381, 503–505, 1996. 962
- Govin, A., Varma, V., and Prange, M.: Astronomically forced vari-  
 ations in western African rainfall (21° N–20° S) during the Last  
 Interglacial period, *Geophys. Res. Lett.*, 41, 2117–2125, doi:  
 10.1002/2013G1058999, 2014.
- Handiani, D., Paul, A., Prange, M., Merkel, U., Dupont, L., and  
 Zhang, X.: Tropical vegetation response to Heinrich Event 1  
 as simulated with the UVic ESCM and CCSM3, *Clim. Past*, 9,  
 1683–1696, doi: 10.5194/cp-9-1683-2013, 2013.
- Hays, J. D., Imbrie, J., and Shackleton, N. J.: Variations in the  
 Earth's orbit: pacemaker of the Ice Ages, *Science*, 194, 1121–  
 1132, 1976.
- Herold, N., Yin, Q. Z., Karami, M. P., and Berger, A.: Modelling  
 the climatic diversity of the warm interglacials, *Quat. Sci. Rev.*,  
 56, 126–141, doi: 10.1016/j.quascirev.2012.08.020, 2012.
- Hessler, I., Harrison, S. P., Kucera, M., Waelbroeck, C., Chen, M.-  
 T., Anderson, C., de Vernal, A., Fréchet, B., Cloke-Hayes, A.,  
 Leduc, G., and Londeix, L.: Implication of methodological un-  
 certainties for mid-Holocene sea surface temperature reconstruc-  
 tions, *Clim. Past*, 10, 2237–2252, doi: 10.5194/cp-10-2237-  
 2014, 2014.
- Hoelzmann, P., Jolly, D., Harrison, S. P., Laarif, F., Bonnefille, R.,  
 and Pachur, H. J.: Mid-Holocene land surface conditions in  
 northern Africa and the Arabian Peninsula: a data set for the  
 analysis of biogeochemical feedbacks in the climate system,  
*Global Biogeochem. Cy.*, 12, 35–52, 1998.
- IPCC: Climate Change 2001: The Scientific Basis. Contribution of  
 Working Group I to the Third Assessment Report of the Inter-  
 governmental Panel on Climate Change [Houghton, J.T., Ding,  
 Y., Griggs, D. J., Noguer, M., van der Linden, P. J., Dai, X.,  
 Maskell, K., and Johnson, C. A., (eds.)], Cambridge University  
 Press, Cambridge, United Kingdom and New York, NY, USA,  
 881pp, 2001.
- Jochum, M., Jahn, A., Peacock, S., Bailey, D. A., Fasullo, J. T.,  
 Kay, J., Levis, S., and Otto-Bliesner, B.: True to Milankovitch:  
 glacial inception in the new Community Climate System  
 Model, *J. Climate*, 25, 2226–2239, doi: 10.1175/JCLI-D-11-  
 00044.1, 2012.
- Jouzel, J., Masson-Delmotte, V., Cattani, O., Dreyfus, G.,  
 Falourd, S., Hoffmann, G., Minster, B., Nouet, J., Barnola, J. M.,  
 Chappellaz, J., Fischer, H., Gallet, J. C., Johnsen, S., Leuen-  
 berger, M., Louergue, L., Luethi, D., Oerter, H., Parrenin, F.,  
 Raisbeck, G., Raynaud, D., Schilt, A., Schwander, J., Selmo, E.,  
 Souchez, R., Spahni, R., Stauffer, B., Steffensen, J. P., Stenni, B.,  
 Stocker, T. F., Tison, J. L., Werner, M., and Wolff, E. W.: Climate  
 variability over the past 800 000 years, *Science*, 317, 793–796,  
 doi: 10.1126/science.1141038, Data archived at the World Data  
 Center for Paleoclimatology, Boulder, Colorado, USA, 2007.
- Joussaume, S. and Braconnot, P.: Sensitivity of paleoclimate simu-  
 lation results to season definitions, *J. Geophys. Res.*, 102, 1943–  
 1956, 1997.
- Kaspar, F. and Cubasch, U.: Simulation of the Eemian interglacial  
 and possible mechanisms for the glacial inception, *Geol. S. Am.*  
 S., 426, 29–41, 2007.
- Khodri, M., Cane, M. A., Kukla, G., Gavin, J., and Braconnot, P.:  
 The impact of precession changes on the Arctic climate during  
 the last interglacial-glacial transition, *Earth Planet. Sc. Lett.*, 236,  
 285–304, 2005.
- Kleinen, T., Hildebrandt, S., Prange, M., Rachmayani, R.,  
 Müller, S., Bezrukova, S., Brovkin, V., and Tarasov, P.: The cli-

- 963 mate and vegetation of Marine Isotope Stage 11 - model results<sup>1022</sup>  
 964 and proxy-based reconstructions at global and regional scale,<sup>1023</sup>  
 965 *Quatern. Int.*, 348, 247–265, doi: 10.1016/j.quaint.2013.12.028,<sup>1024</sup>  
 966 2014. <sup>1025</sup>
- 967 Kopp, R. E., Simons, F. J., Mitrovica, J. X., Maloof, A. C., and<sup>1026</sup>  
 968 Oppenheimer, M.: Probabilistic assessment of sea level during<sup>1027</sup>  
 969 the last interglacial stage. *Nature*, 462(7275), 863–868, 2009. <sup>1028</sup>
- 970 Kroon, D., Alexander, I., Little, M., Lourens, L. J., Matthewson, A.,<sup>1029</sup>  
 971 Robertson, A. H., and Sakamoto, T.: Oxygen isotope and sapro-<sup>1030</sup>  
 972 pel stratigraphy in the eastern Mediterranean during the last 3.2<sup>1031</sup>  
 973 million years, *Proceedings of the Ocean Drilling Program, Sci-*<sup>1032</sup>  
 974 *entific Results*, 160, 181–189, 1998. <sup>1033</sup>
- 975 Kubatzki, C., Montoya, M., Rahmstorf, S., Ganopolski, A.,<sup>1034</sup>  
 976 Claussen, M.: Comparison of a coupled global model of interme-<sup>1035</sup>  
 977 diate complexity and an AOGCM for the last interglacial, *Clim.*<sup>1036</sup>  
 978 *Dyn.*, 16, 799–814, 2000. <sup>1037</sup>
- 979 Lang, N. and Wolff, E. W.: Interglacial and glacial variability from<sup>1038</sup>  
 980 the last 800 kyr in marine, ice and terrestrial archives, *Clim. Past*,<sup>1039</sup>  
 981 7, 361–380, doi:10.5194/cp-7-361-2011, 2011. <sup>1040</sup>
- 982 Levis, S., Bonan, G. B., Vertenstein, M., and Oleson, K. W.: The<sup>1041</sup>  
 983 Community Land Models Dynamic Global Vegetation Model<sup>1042</sup>  
 984 (CLM-DGVM): Technical Description and User’s Guide, NCAR<sup>1043</sup>  
 985 Technical Note NCAR/TN-459+IA, National Center for Atmo-<sup>1044</sup>  
 986 spheric Research, Boulder, CO, 2004. <sup>1045</sup>
- 987 Lisiecki, L. E. and Raymo, M. E.: A Pliocene-Pleistocene stack of 57<sup>1046</sup>  
 988 globally distributed benthic  $\delta^{18}\text{O}$  records, *Paleoceanography*, 20,<sup>1047</sup>  
 989 PA1003, doi: 10.1029/2004PA001071, 2005. <sup>1048</sup>
- 990 Liu, Z., Zhu, J., Rosenthal, Y., Zhang, X., Otto-Bliesner, B. L.,<sup>1049</sup>  
 991 Timmermann, A., Smith, R. S., Lohmann, G., Zheng, W.,<sup>1050</sup>  
 992 and Timm, O. E.: The Holocene temperature conun-<sup>1051</sup>  
 993 drum, *P. Natl. Acad. Sci. USA*, 111, E3501–E3505, doi:<sup>1052</sup>  
 994 10.1073/pnas.1407229111, 2014. <sup>1053</sup>
- 995 Lohmann, G., Pfeiffer, M., Laepple, T., Leduc, G., and Kim, J.-<sup>1054</sup>  
 996 H.: A model–data comparison of the Holocene global sea sur-<sup>1055</sup>  
 997 face temperature evolution, *Clim. Past*, 9, 1807–1839, doi:<sup>1056</sup>  
 998 10.5194/cp-9-1807-2013, 2013. <sup>1057</sup>
- 999 Lorenz, S. J. and Lohmann, G.: Acceleration technique for Mi-<sup>1058</sup>  
 1000 lankovitch type forcing in a coupled atmosphere–ocean circu-<sup>1059</sup>  
 1001 lation model: method and application for the Holocene, *Clim.*<sup>1060</sup>  
 1002 *Dyn.*, 23, 727–743, 2004. <sup>1061</sup>
- 1003 Loulergue, L., Schilt, A., Spahni, R., Masson-Delmotte, V., Blu-<sup>1062</sup>  
 1004 nier, T., Lemieux, B., Barnola, J.-M., Raynaud, D., Stocker, T. F.,<sup>1063</sup>  
 1005 and Chappellaz, J.: Orbital and millennial-scale features of atmo-<sup>1064</sup>  
 1006 spheric  $\text{CH}_4$  over the past 800,000 years, *Nature*, 453, 383–386,<sup>1065</sup>  
 1007 2008. <sup>1066</sup>
- 1008 Loutre, M. F., and Berger, A.: Marine Isotope Stage 11 as an ana-<sup>1067</sup>  
 1009 logue for the present interglacial, *Global and Planetary Change*,<sup>1068</sup>  
 1010 36(3), 209–217, 2003. <sup>1069</sup>
- 1011 Lunt, D. J., Abe-Ouchi, A., Bakker, P., Berger, A., Braconnot, P.,<sup>1070</sup>  
 1012 Charbit, S., Fischer, N., Herold, N., Jungclaus, J. H., Khon, V. C.,<sup>1071</sup>  
 1013 Krebs-Kanzow, U., Langebroek, P. M., Lohmann, G., Nisan-<sup>1072</sup>  
 1014 cioglu, K. H., Otto-Bliesner, B. L., Park, W., Pfeiffer, M.,<sup>1073</sup>  
 1015 Phipps, S. J., Prange, M., Rachmayani, R., Renssen, H., Rosen-<sup>1074</sup>  
 1016 bloom, N., Schneider, B., Stone, E. J., Takahashi, K., Wei, W.,<sup>1075</sup>  
 1017 Yin, Q., and Zhang, Z. S.: A multi-model assessment of last in-<sup>1076</sup>  
 1018 terglacial temperatures, *Clim. Past*, 9, 699–717, doi: 10.5194/cp-<sup>1077</sup>  
 1019 9-699-2013, 2013. <sup>1078</sup>
- 1020 Lüthi, D., Le Floch, M., Bereiter, B., Blunier, T., Barnola, J.-M.,<sup>1079</sup>  
 1021 Siegenthaler, U., Raynaud, D., Jouzel, J., Fischer, H., Kawa-<sup>1080</sup>
- mura, K., and Stocker, T. F.: High-resolution carbon dioxide con-  
 centration record 650,000–800,000 years before present, *Nature*,  
 453, 379–382, 2008.
- Mantsis, D. F., Clement, A. C., Broccoli, A. J., and Erb, M. P.: Cli-  
 mate feedbacks in response to changes in obliquity, *J. Climate*,  
 24, 2830–2845, 2011.
- Mantsis, D. F., Lintner, B. R., Broccoli, A. J., Erb, M. P.,  
 Clement, A. C., and Park, H. S.: The response of large-scale  
 circulation to obliquity-induced changes in meridional heating  
 gradients, *J. Climate*, 27, 5504–5516, 2014.
- Marzin, C., Braconnot, P., and Kageyama, M.: Relative impacts  
 of insolation changes, meltwater fluxes and ice sheets on African  
 and Asian monsoons during the Holocene, *Clim. Dyn.*, 41, 2267–  
 2286, 2013.
- McClure, H. A.: Radiocarbon chronology of late Quaternary lakes  
 in the Arabian Desert, *Nature*, 263, 755–756, 1976.
- Meissner, K. J., Weaver, A. J., Matthews, H. D., and Cox, P. M.: The  
 role of land-surface dynamics in glacial inception: a study with  
 the UVic Earth System Climate Model, *Clim. Dyn.*, 21, 519–537,  
 2003.
- Milker, Y., Rachmayani, R., Weinkauff, M. F. G., Prange, M.,  
 Raitzsch, M., Schulz, M., and Kučera, M.: Global and regional  
 sea surface temperature trends during Marine Isotope Stage 11,  
*Clim. Past*, 9, 2231–2252, doi: 10.5194/cp-9-2231-2013, 2013.
- Murray-Wallace, C., V.: Pleistocene coastal stratigraphy, sealevel  
 highstands and neotectonism of the southern Australian pas-  
 sive continental margin a review, *Journal of Quaternary Science*,  
 17(5–6), 469–489., 2002.
- Muri, H., Berger, A., Yin, Q., Karami, M., and Barriat, P. V.: The  
 climate of the MIS-13 Interglacial according to HadCM3, *J. Cli-  
 mate*, 26, 9696–9712, 2013.
- Nikolova, I., Yin, Q., Berger, A., Singh, U. K., and Karami, M. P.:  
 The last interglacial (Eemian) climate simulated by LOVECLIM  
 and CCSM3, *Clim. Past*, 9, 1789–1806, doi: 10.5194/cp-9-1789-  
 2013, 2013.
- Oleson, K. W., Niu, G. Y., Yang, Z. L., Lawrence, D. M., Thorn-  
 ton, P. E., Lawrence, P. J., Stockli, R., Dickinson, R. E. G.,  
 Bonan, B., Levis, S., Dai, A., and Qian, T.: Improve-  
 ments to the Community Land Model and their impact on  
 the hydrological cycle, *J. Geophys. Res.*, 113, G01021, doi:  
 10.1029/2007JG000563, 2008.
- Otto-Bliesner, B. L., Tomas, R., Brady, E. C., Ammann, C.,  
 Kothavala, Z., and Clauzet, G.: Climate sensitivity of moder-  
 ate and low-resolution versions of CCSM3 to preindustrial forc-  
 ings, *J. Climate*, 19, 2567–2583, 2006.
- Otto-Bliesner, B. L., Rosenbloom, N., Stone, E. J., McKay,  
 N. P., Lunt, D. J., Brady, E. C., Overpeck, J. T.: How  
 warm was the last interglacial? New model-data comparisons,  
*Philos. Trans. R. Soc. London Ser. A*, 371, 20130097, doi:  
 10.1098/rsta.2013.0097; pmid: 24043870, 2013.
- Prell, W. L. and Kutzbach, J. E.: Monsoon variability over the past  
 150,000 years, *J. Geophys. Res.*, 92, 8411–8425, 1987.
- Rachmayani, R., Prange, M., and Schulz, M.: North African  
 vegetation–precipitation feedback in early and mid-Holocene cli-  
 mate simulations with CCSM3-DGVM, *Clim. Past*, 11, 175–185,  
 doi: 10.5194/cp-11-175-2015, 2015.
- Raymo, M. E., Nisancioglu, K. H.: The 41 kyr world: Mi-  
 lankovitch’s other unsolved mystery, *Paleoceanography*, 18 (1),  
 1011, doi: 10.1029/2002PA000791, 2003.

- 1081 Raymo, M. E., Mitrovica, J. X.: Collapse of polar ice sheets during  
1082 the stage 11 interglacial, *Nature*, 2012/03/22/print, 483, 7390,  
1083 453–456, 2012. 1140–1142
- 1084 Renssen, H., Driesschaert, E., Loutre, M.F., Fichefet, T.: On the  
1085 importance of initial conditions for simulations of the Mid-  
1086 Holocene climate. *Clim. Past*, 2, 91–97, 2006. 1143–1145
- 1087 Renssen, H., Seppä, H., Heiri, O., Roche, D. M., Goosse, H.,  
1088 and Fichefet, T.: The spatial and temporal complexity of the  
1089 Holocene thermal maximum, *Nat. Geosci.*, 2, 411–414, 2009. 1146–1148
- 1090 Schilt, A., Baumgartner, M., Blunier, T., Schwander, J., Spahni, R.,  
1091 Fischer, H., and Stocker, T. F.: Glacial–interglacial and  
1092 millennial–scale variations in the atmospheric nitrous oxide con-  
1093 centration during the last 800.000 years, *Quat. Sci. Rev.*, 29, 182–  
1094 192, 2010. 1149–1153
- 1095 Sitch, S., Smith, B., Prentice, I. C., Arneeth, A., Bondeau, A.,  
1096 Cramer, W., Kaplan, J. O., Levis, S., Lucht, W., Sykes, M. T.,  
1097 Thonicke, K., and Venevsky, S.: Evaluation of ecosystem dy-  
1098 namics, plant geography and terrestrial carbon cycling in the  
1099 LPJ dynamic vegetation model, *Glob. Change Biol.*, 9, 161–185,  
1100 2003.
- 1101 Tiedemann, R., Sarnthein, M., and Shackleton, N. J.: Astronomic  
1102 timescale for the Pliocene Atlantic  $\delta^{18}\text{O}$  and dust flux records  
1103 of Ocean Drilling Program Site 659, *Paleoceanography*, 9, 619–  
1104 638, 1994.
- 1105 Timm, O., Timmermann, A., Abe-Ouchi, A., Saito, F., and  
1106 Segawa, T.: On the definition of seasons in paleoclimate sim-  
1107 ulations with orbital forcing, *Paleoceanography*, 23, PA2221,  
1108 doi:10.1029/2007PA001461, 2008.
- 1109 Trenberth, K. E., Stepaniak, D. P., and Caron, J. M.: The global  
1110 monsoon as seen through the divergent atmospheric circula-  
1111 tion, *J. Climate*, 13, 3969–3993, 2000.
- 1112 Tuenter, E., Weber, S., Hilgen, F., and Lourens, L.: The response of  
1113 the African boreal summer monsoon to remote and local forcing  
1114 due to precession and obliquity, *Global Planet. Change*, 36, 219–  
1115 235, 2003.
- 1116 Tzedakis, P. C., Hooghiemstra, H., and Palike, H.: The last 1.35  
1117 million years at Tenaghi Philippon: revised chronostratigraphy  
1118 and long-term vegetation trends, *Quat. Sci. Rev.*, 25, 3416–3430,  
1119 2006.
- 1120 Tzedakis, P. C., Raynaud, D., McManus, J. F., Berger, A.,  
1121 Brovkin, V., and Kiefer, T.: Interglacial diversity, *Nat. Geosci.*,  
1122 2, 751–755, 2009.
- 1123 van Nes, E. H., Scheffer, M., Brovkin, V., Lenton, T. M., Ye, H.,  
1124 Deyle, E., and Sugihara, G.: Causal feedbacks in climate change,  
1125 *Nature Climate Change*, 5, 445–448, doi: 10.1038/nclimate2568,  
1126 2015.
- 1127 Varma, V., Prange, M., Merkel, U., Kleinen, T., Lohmann, G., Pfeif-  
1128 fer, M., Renssen, H., Wagner, A., Wagner, S., and Schulz, M.:  
1129 Holocene evolution of the Southern Hemisphere westerly winds  
1130 in transient simulations with global climate models, *Clim. Past*,  
1131 8, 391–402, doi: 10.5194/cp-8-391-2012, 2012.
- 1132 Wang, P. X., Wang, B., Cheng, H., Fasullo, J., Guo, Z. T., Kiefer, T.,  
1133 and Liu, Z. Y.: The global monsoon across timescales: coherent  
1134 variability of regional monsoons, *Clim. Past*, 10, 2007–2052,  
1135 doi: 10.5194/cp-10-2007-2014, 2014.
- 1136 Yeager, S. G., Shields, C. A., Large, W. G., and Hack, J. J.: The  
1137 low-resolution CCSM3, *J. Climate*, 19, 2545–2566, 2006.
- 1138 Yin Q. Z., and Berger, A.: Interglacial analogues of the Holocene  
1139 and its natural near future, *Quat. Sci. Rev.*, 20, 2015.
- Yin, Q. Z. and Berger, A.: Individual contribution of insolation and  
CO<sub>2</sub> to the interglacial climates of the past 800,000 years, *Clim.  
Dyn.*, 38, 709–724, 2012.
- Yin, Q., Berger, A., Driesschaert, E., Goosse, H., Loutre, M. F.,  
and Crucifix, M.: The Eurasian ice sheet reinforces the East  
Asian summer monsoon during the interglacial 500 000 years  
ago, *Clim. Past*, 4, 79–90, doi: 10.5194/cp-4-79-2008, 2008.
- Yin, Q. Z., Berger, A., and Crucifix, M.: Individual and combined  
effects of ice sheets and precession on MIS-13 climate, *Clim.  
Past*, 5, 229–243, doi: 10.5194/cp-5-229-2009, 2009.
- Yin, Q. Z. and Berger, A.: Insolation and CO<sub>2</sub> contribution to the  
interglacial climate before and after the Mid-Brunhes Event, *Nat.  
Geosci.* 3, 243–246, doi: 10.1038/ngeo771, 2010.
- Zheng, W. and Braconnot, P.: Characterization of Model Spread in  
PMIP2 Mid-Holocene Simulations of the African Monsoon, *J.  
Climate*, 26, 1192–1210, 2013.

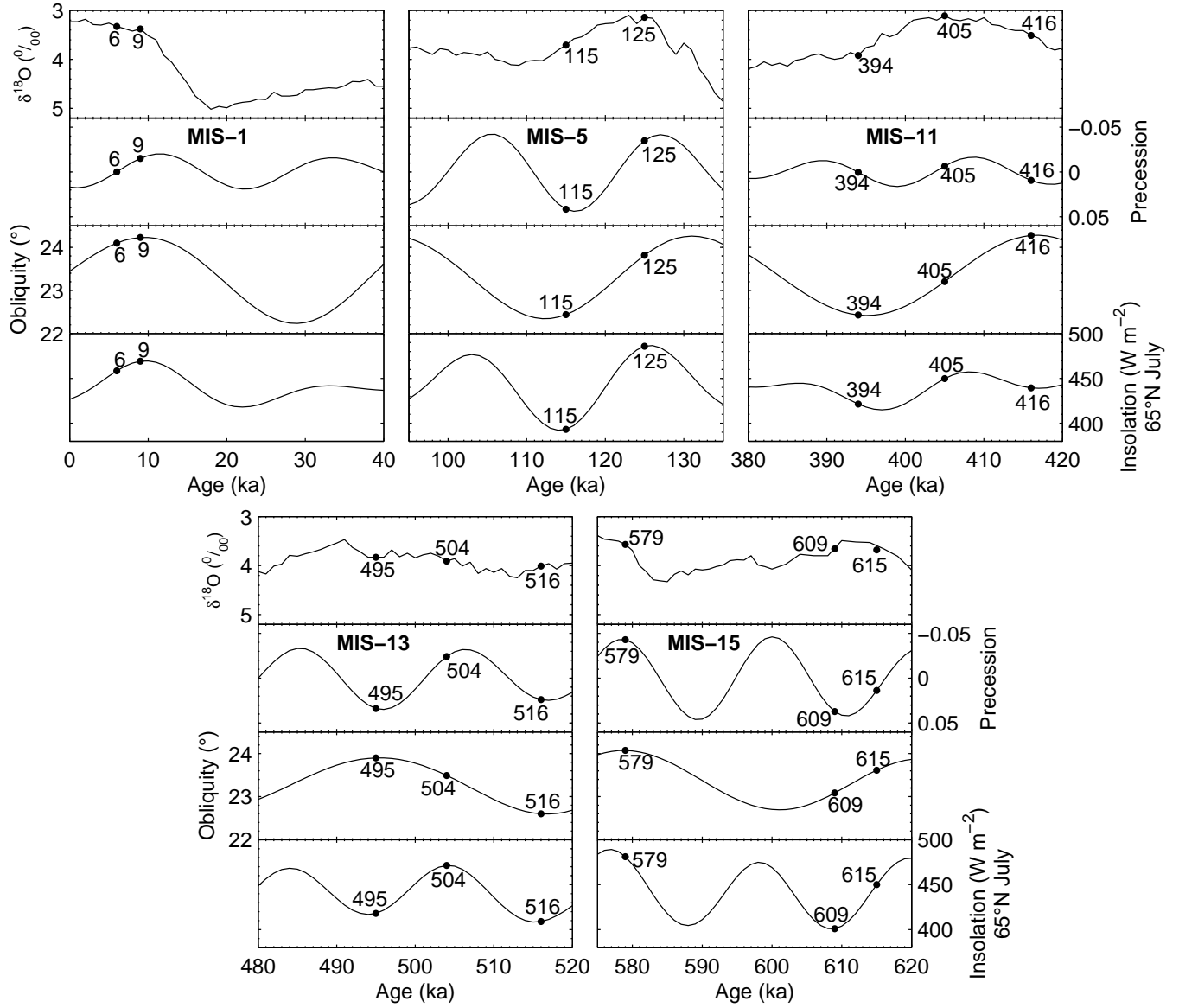


**Figure 1.** Benthic  $\delta^{18}\text{O}$  stack (Lisiecki and Raymo, 2005), climatic precession, obliquity, and insolation at July,  $65^\circ\text{N}$  (Berger, 1978) for the different interglacials. The points mark the time slices simulated in this study.

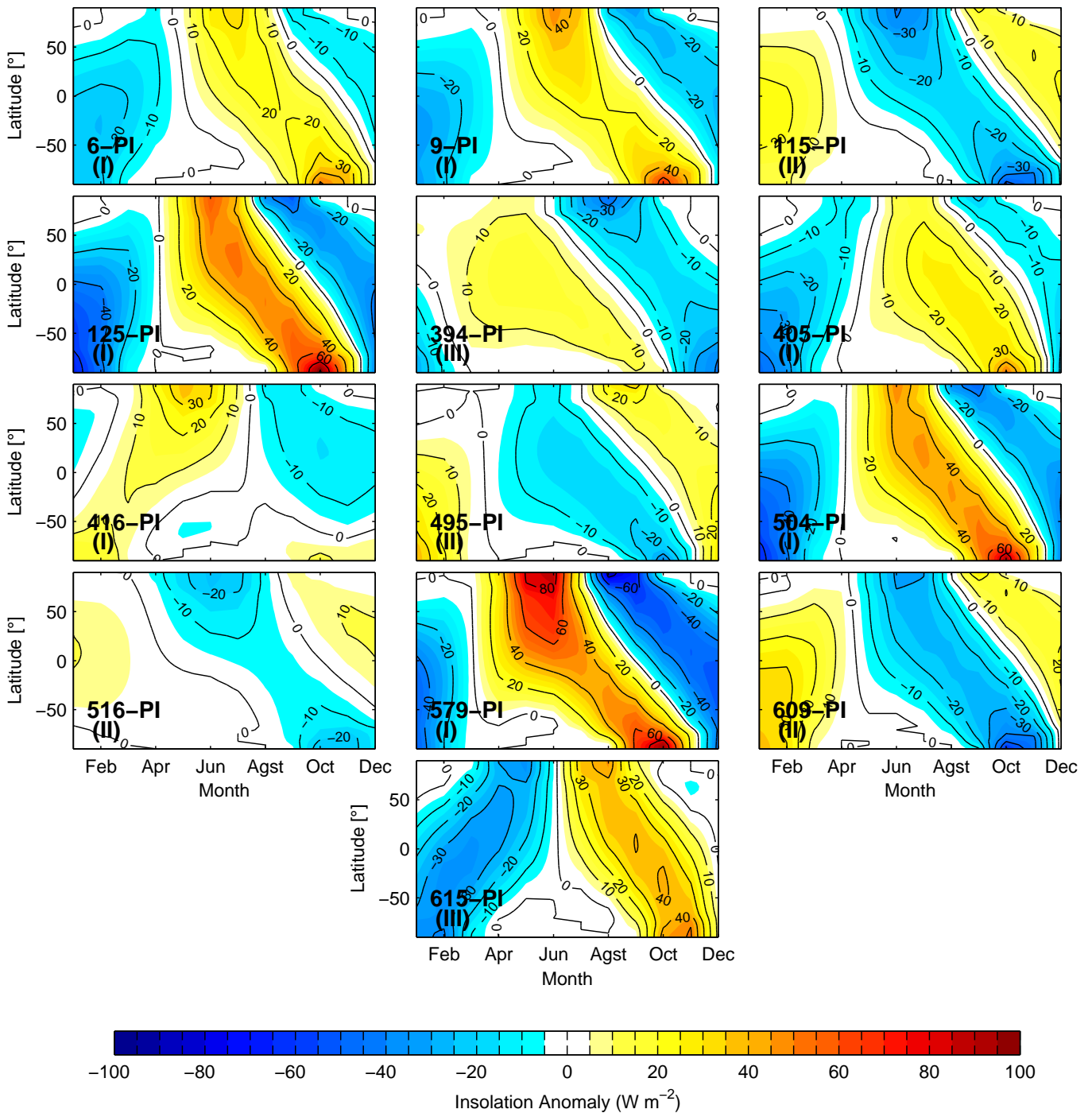


**Figure 2.** Insolation anomalies (relative to PI) for the time slices simulated in this study. Patterns of insolation anomaly are classified into Groups I, II, and III (see text). The calculation assumes a fixed present-day calendar with vernal equinox at 21 March.

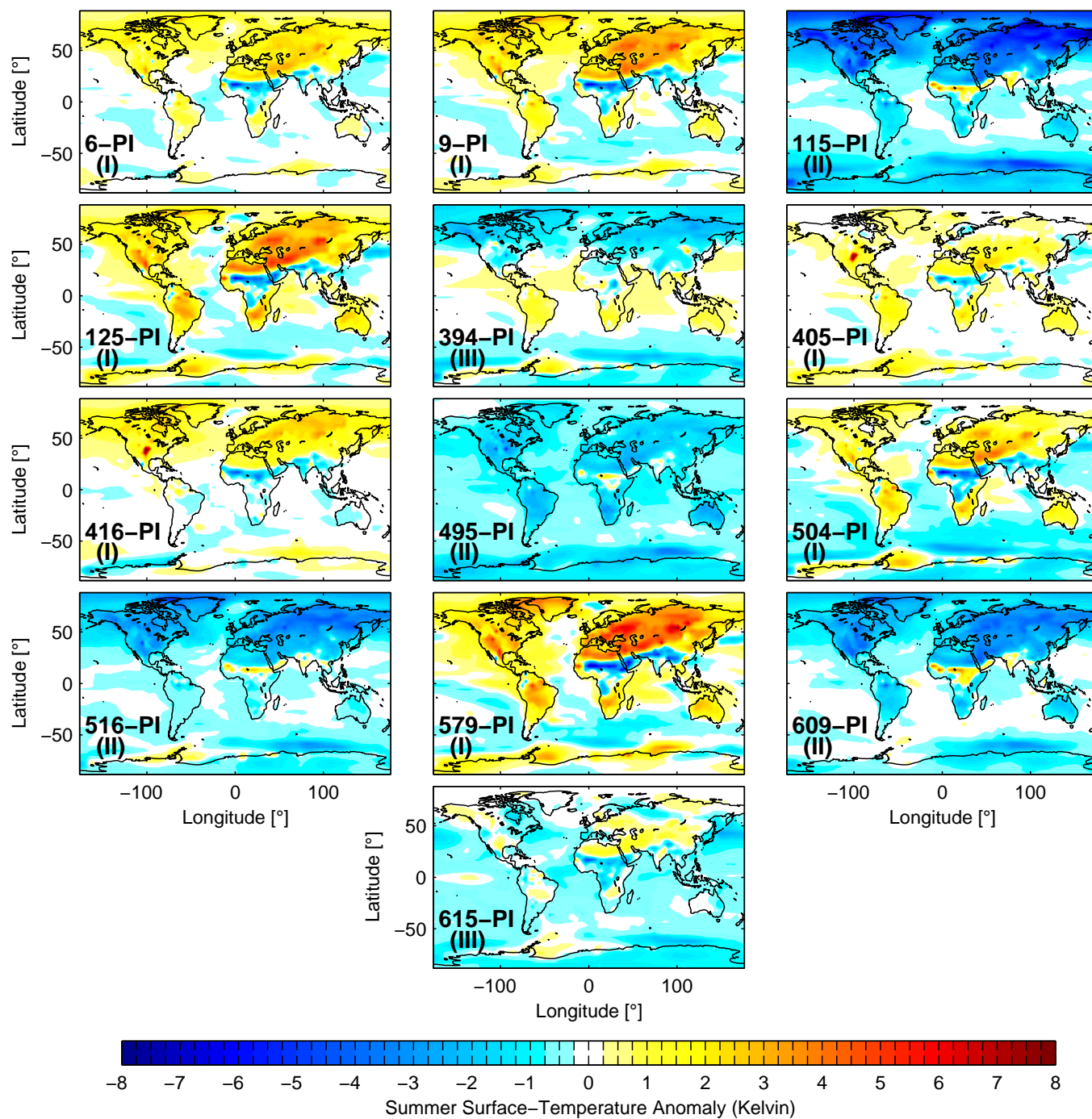


**Figure 3.** Boreal summer surface temperature anomalies (relative to PI) for the different interglacial time slices. Classification into Groups I, II, and III (see text) is indicated.

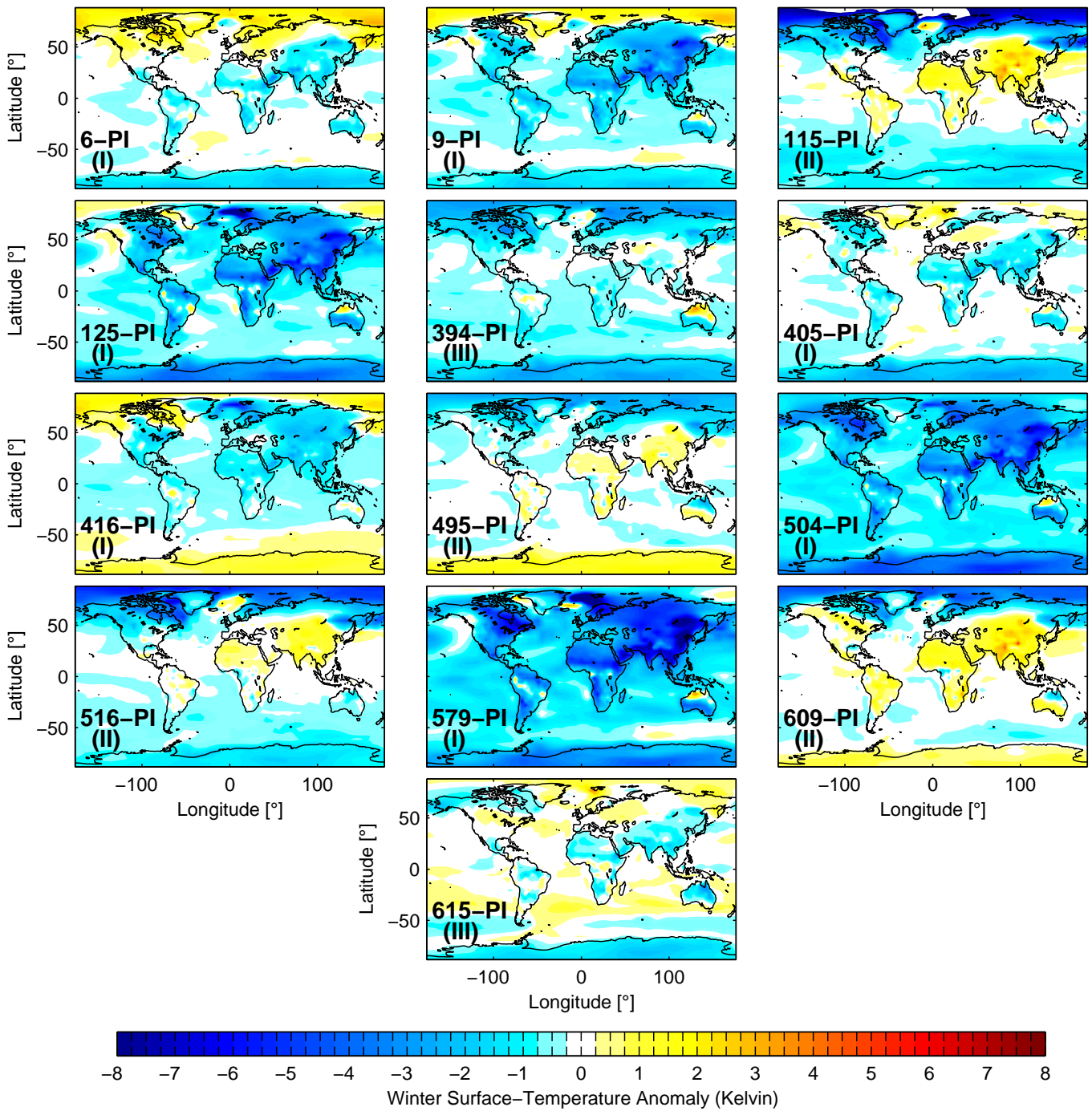


**Figure 4.** As in Fig. 3, but for boreal winter.

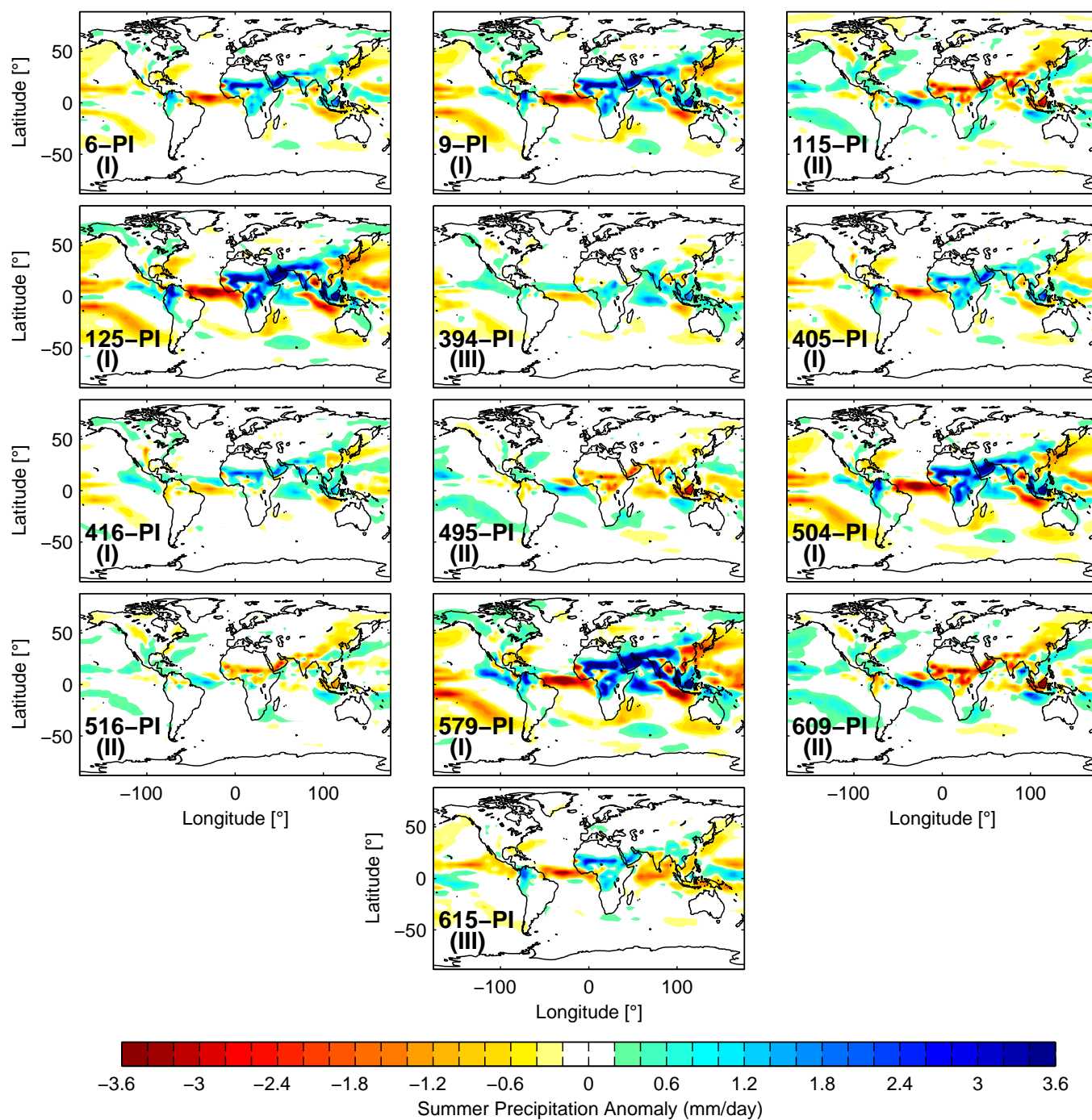
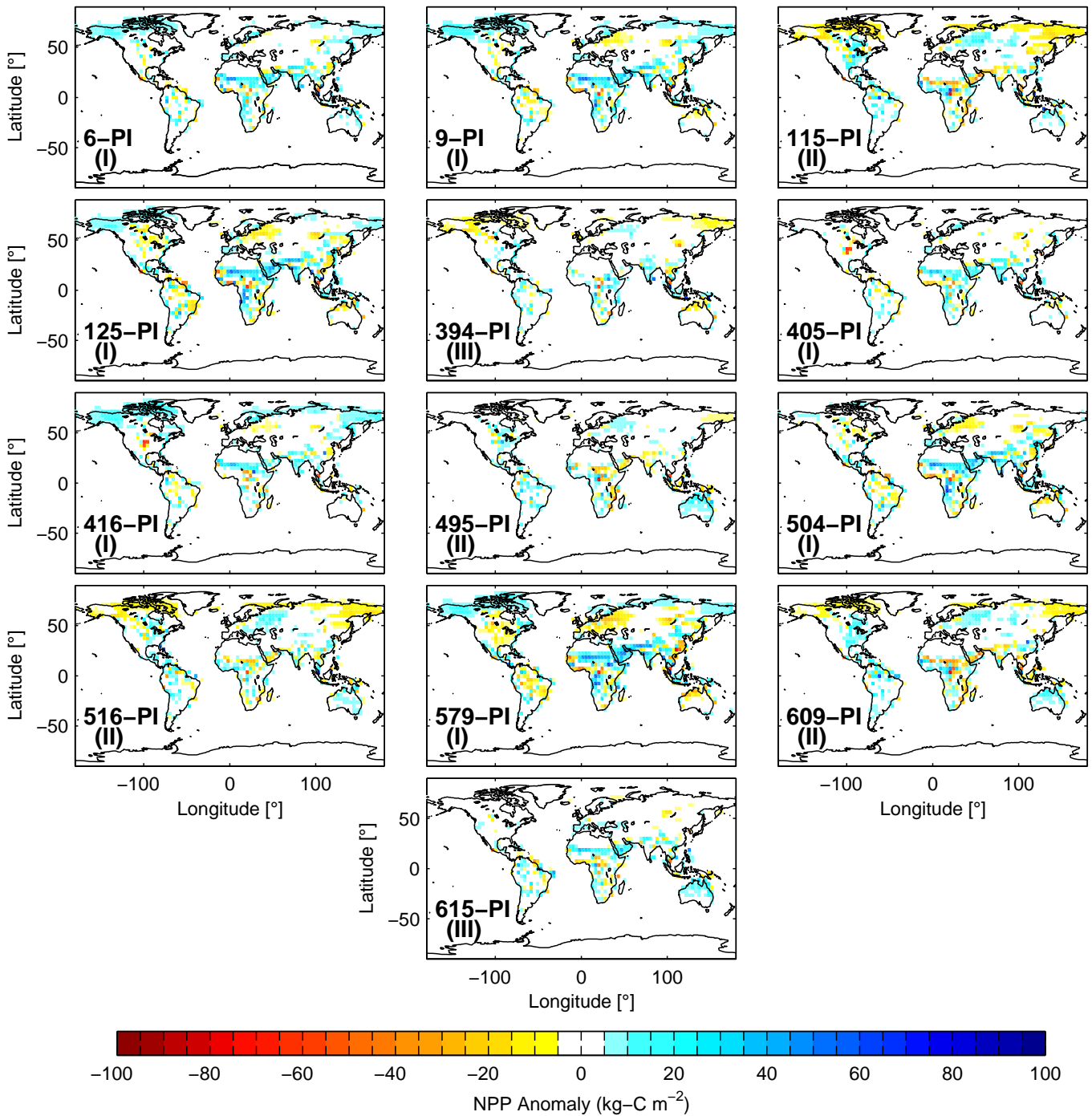
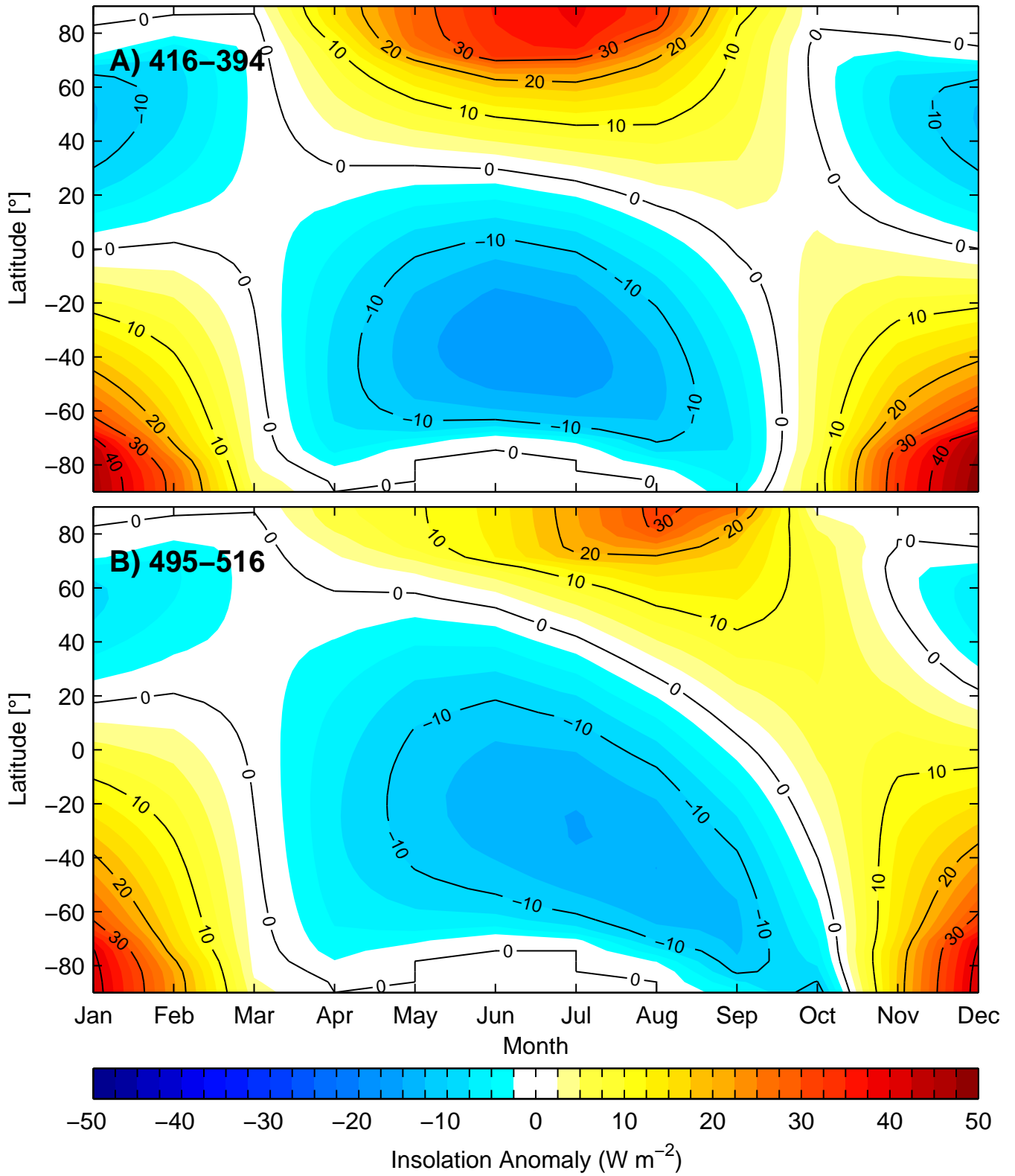


Figure 5. As in Fig. 3, but for boreal summer precipitation.





**Figure 6.** As in Fig. 3, but for annual net primary production.



**Figure 7.** Differences in the seasonal and latitudinal distribution of insolation for (A) 416-394 ka BP, (B) 495-516 ka BP.

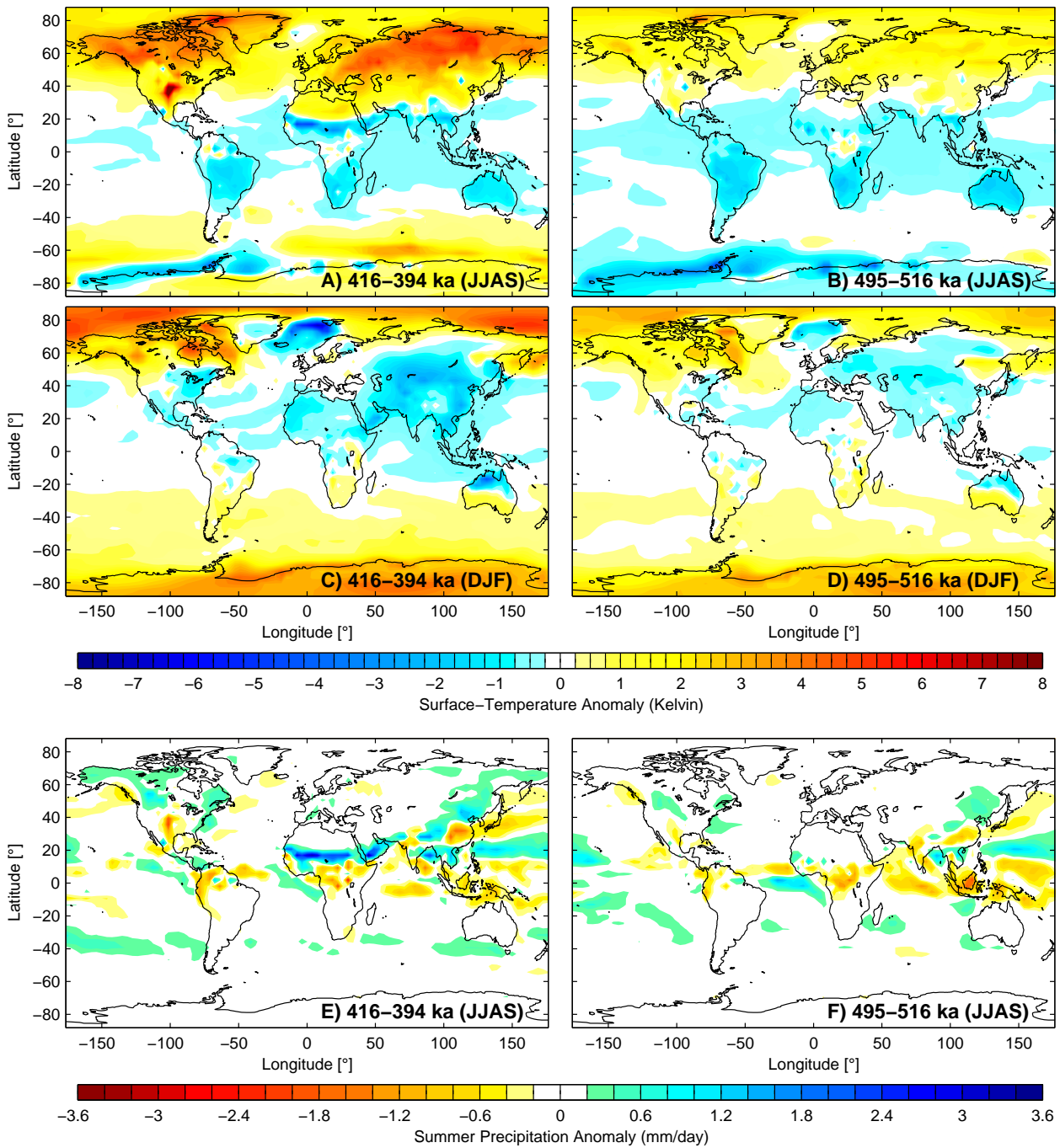


**Figure 8.** Differences in seasonal surface temperature (A)–(D) and boreal summer precipitation (E)–(F) for 416–394 ka BP (left) and 495–516 ka BP (right).

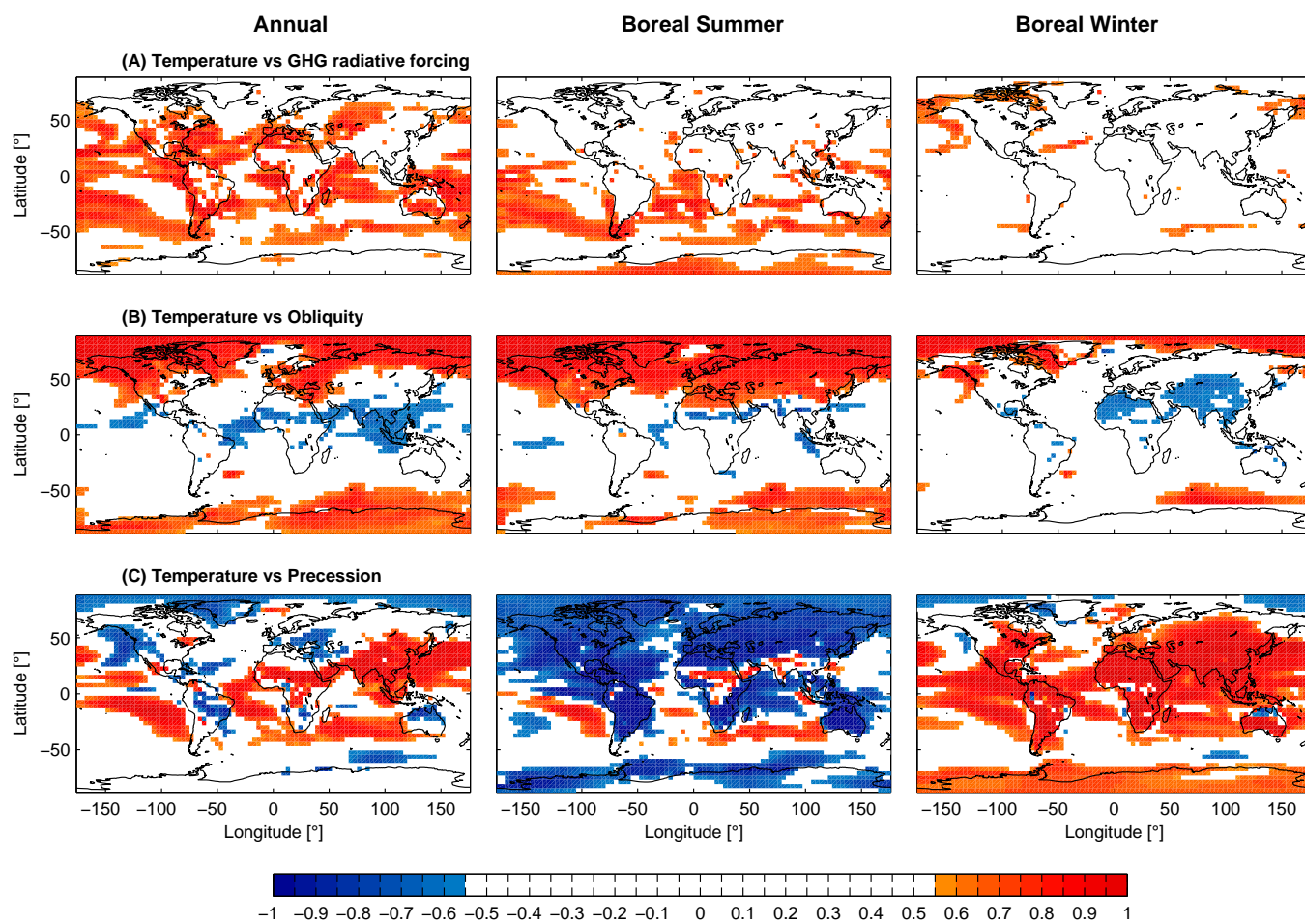


**Figure 9.** Linear correlation maps between surface temperature and GHG radiative forcing (A), obliquity (B), and climatic precession (C) as calculated from the entire set of experiments. Summer refers to JJAS, winter to DJF. Only significant values are shown according to a two-sided Student’s t-test at 95% confidence level.

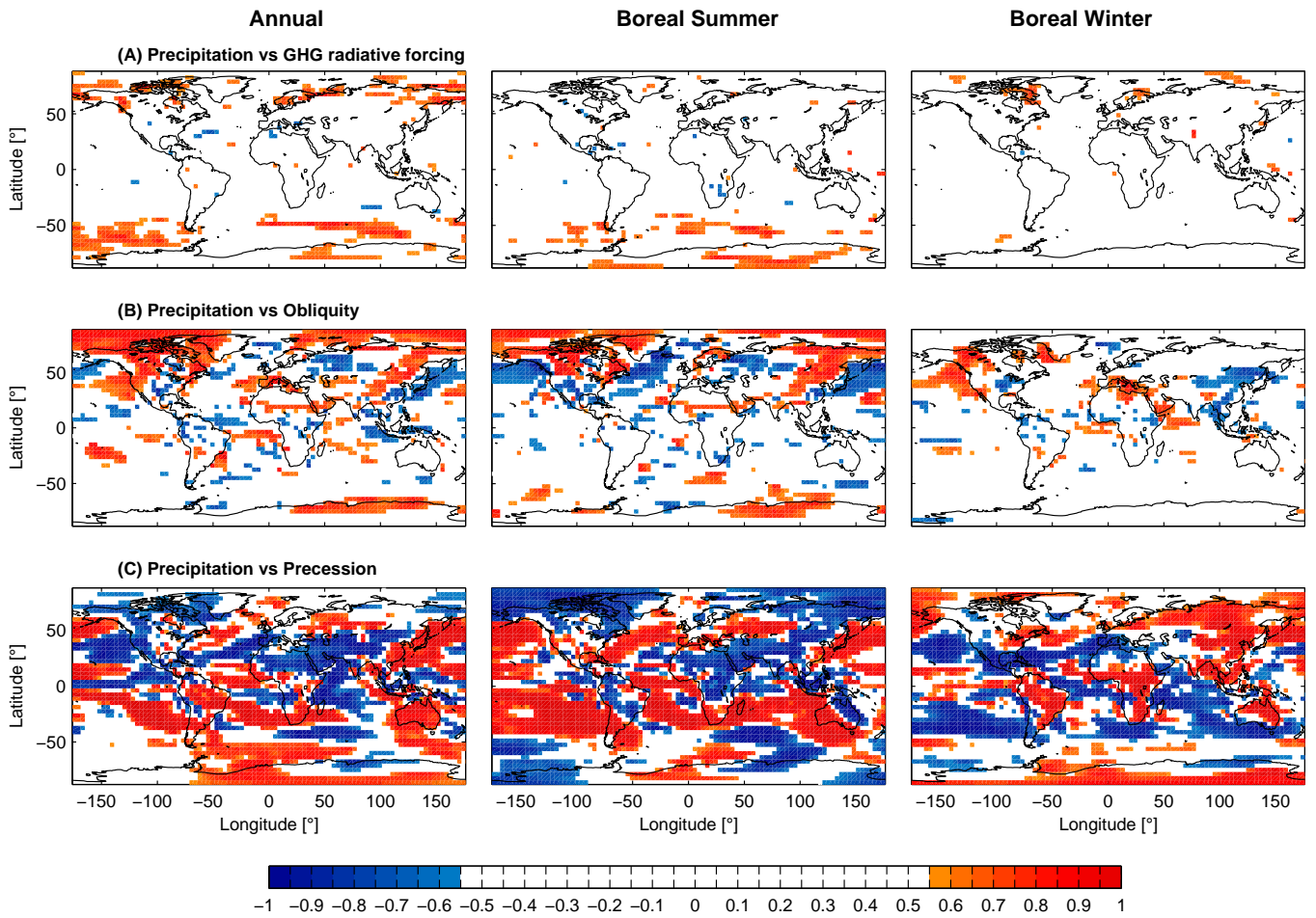


Figure 10. As in Fig. 9, but for precipitation.